ORIGINAL ARTICLE

Inherited DOCK2 Deficiency in Patients with Early-Onset Invasive Infections

K. Dobbs, C. Domínguez Conde, S.-Y. Zhang, S. Parolini, M. Audry, J. Chou, E. Haapaniemi, S. Keles, I. Bilic, S. Okada, M.J. Massaad, S. Rounioja, A.M. Alwahadneh, N.K. Serwas, K. Capuder, E. Çiftçi, K. Felgentreff, T.K. Ohsumi, V. Pedergnana, B. Boisson, Ş. Haskoloğlu, A. Ensari, M. Schuster, A. Moretta, Y. Itan, O. Patrizi, F. Rozenberg, P. Lebon, J. Saarela, M. Knip, S. Petrovski, D.B. Goldstein, R.E. Parrott, B. Savas, A. Schambach, G. Tabellini, C. Bock, T.A. Chatila, A.M. Comeau, R.S. Geha, L. Abel, R.H. Buckley, A. İkincioğulları, W. Al-Herz, M. Helminen, F. Doğu, J.-L. Casanova, K. Boztuğ, and L.D. Notarangelo

ABSTRACT

BACKGROUND

Combined immunodeficiencies are marked by inborn errors of T-cell immunity in which the T cells that are present are quantitatively or functionally deficient. Impaired humoral immunity is also common. Patients have severe infections, autoimmunity, or both. The specific molecular, cellular, and clinical features of many types of combined immunodeficiencies remain unknown.

METHODS

We performed genetic and cellular immunologic studies involving five unrelated children with early-onset invasive bacterial and viral infections, lymphopenia, and defective T-cell, B-cell, and natural killer (NK)–cell responses. Two patients died early in childhood; after allogeneic hematopoietic stem-cell transplantation, the other three had normalization of T-cell function and clinical improvement.

RESULTS

We identified biallelic mutations in the dedicator of cytokinesis 2 gene (*DOCK2*) in these five patients. RAC1 activation was impaired in the T cells. Chemokine-induced migration and actin polymerization were defective in the T cells, B cells, and NK cells. NK-cell degranulation was also affected. Interferon-α and interferon-λ production by peripheral-blood mononuclear cells was diminished after viral infection. Moreover, in DOCK2-deficient fibroblasts, viral replication was increased and virus-induced cell death was enhanced; these conditions were normalized by treatment with interferon alfa-2b or after expression of wild-type *DOCK2*.

CONCLUSIONS

Autosomal recessive DOCK2 deficiency is a new mendelian disorder with pleiotropic defects of hematopoietic and nonhematopoietic immunity. Children with clinical features of combined immunodeficiencies, especially with early-onset, invasive infections, may have this condition. (Supported by the National Institutes of Health and others.)

The authors' full names, academic degrees, and affiliations are listed in the Appendix. Address reprint requests to Dr. Notarangelo at the Division of Immunology, Boston Children's Hospital, Karp Research Bldg., Rm. 10217, 1 Blackfan Circle, Boston, MA 02115, or at luigi.notarangelo@childrens.harvard.edu; Dr. Zhang at St. Giles Laboratory of Human Genetics of Infectious Disease, Rockefeller University, 1230 York Ave., New York, NY 10065, or at shzh289@mail.rockefeller.edu; Dr. Casanova at St. Giles Laboratory of Human Genetics of Infectious Disease, Rockefeller University, 1230 York Ave., New York, NY 10065, or at casanova@rockefeller.edu; or Dr. Boztuğ at the CeMM Research Center for Molecular Medicine of the Austrian Academy of Sciences and Department of Pediatrics and Adolescent Medicine, Medical University of Vienna, Lazarettgasse 14 AKH BT 25.3, A-1090 Vienna, Austria, or at kboztug@cemm.oeaw.ac.at.

Mr. Dobbs, Ms. Domínguez Conde, Dr. Zhang, and Dr. Parolini, and Drs. Buckley, İkincioğulları, Al-Herz, Helminen, Doğu, Casanova, Boztuğ, and Notarangelo contributed equally to this article.

N Engl J Med 2015;372:2409-22.
DOI: 10.1056/NEJMoa1413462
Copyright © 2015 Massachusetts Medical Society.

The New England Journal of Medicine
Downloaded from nejm.org at Harvard Library on January 31, 2016. For personal use only. No other uses without permission.
Copyright © 2015 Massachusetts Medical Society. All rights reserved.

Combined immunodeficiencies comprise a heterogeneous group of inherited defects of the immune system that are characterized by quantitative or qualitative defects of T lymphocytes. These defects are associated with primary or secondary defects of B lymphocytes.[1] In patients with combined immunodeficiencies, impairment of adaptive immunity causes increased susceptibility to early-onset, severe infections with a variety of viruses, bacteria, fungi, and parasites.[1,2] Autoimmune manifestations, allergies, and cancers can also occur.[2]

Identification of gene defects that cause combined immunodeficiencies has helped patients considerably, provided new and important insights into mechanisms governing T-cell development and function in humans,[2] and led to an understanding of the molecular and cellular basis of common conditions, including autoimmunity, allergy, inflammation, and cancer. However, the specific molecular, cellular, and clinical features of many combined immunodeficiencies remain poorly defined.

Next-generation sequencing has revolutionized studies of human genetic diseases, enabling the identification of new causative genetic variations in an increasing number of patients with primary immunodeficiencies.[3-7] Here we report on human dedicator of cytokinesis 2 (DOCK2) deficiency as a combined immunodeficiency in five unrelated patients of various ethnic origins. These patients presented with a distinctive clinical phenotype of early-onset, invasive infections that were associated with a broad spectrum of defects in hematopoietic and nonhematopoietic immunity.

Figure 1 (facing page). Identification of *DOCK2* Mutations in Patients with Combined Immunodeficiency.

Panel A shows the pedigrees of the five families of the patients with *DOCK2* mutations in the study (Patients 1 through 5, solid symbols). Circles represent female family members, and squares male family members. A slash through a symbol represents a deceased person. Chromatograms corresponding to the identified *DOCK2* mutations in these patients and heterozygous carriers for each family are shown. Panel B shows the clinical spectrum of DOCK2 deficiency (from left to right): pneumonia requiring intubation in Patient 2, rash with vesicular lesions due to varicella in Patient 3, and neutrophil infiltrate in colonic lamina propria and crypt epithelium consistent with focal active colitis in Patient 4 (hematoxylin and eosin, low magnification). Panel C shows the distribution of the identified mutations relative to the DOCK2 protein structure depicting the SRC homology 3 (SH3) domain, the DOCK homology region 1 (DHR-1) domain, and the DOCK homology region 2 (DHR-2) domain. Panel D shows the immunoblot analysis of protein lysates from Epstein–Barr virus (EBV)–transformed B-cell lines from Patient 3 and two healthy controls and protein lysates from T-cell lines from Patients 1 and 2 and a control. Glyceraldehyde-3-phosphate dehydrogenase (GAPDH) served as protein-loading control.

METHODS

STUDY OVERSIGHT

The study was approved by the institutional review boards of the Kuwait Ministry of Health, INSERM, Rockefeller University, the Medical University of Vienna, Ankara University Medical School, Boston Children's Hospital, and Duke University School of Medicine. Written informed consent was obtained from the patients' parents or guardians.

CASE PATIENTS

Pedigrees of the five unrelated index patients are shown in Figure 1A, and Figure S1 in the Supplementary Appendix, available with the full text of this article at NEJM.org. Clinical and laboratory data are summarized in Table 1.

Patient 1, a boy born to consanguineous Lebanese parents, presented at 3 months of age with respiratory syncytial virus bronchiolitis, followed by recurrent episodes of pneumonia. At 5 months of age, severe T-cell lymphopenia and markedly reduced in vitro T-cell proliferation were observed (Table 1). At 9 months of age, after myeloablative conditioning with busulfan and fludarabine, he underwent T-cell–depleted haploidentical hematopoietic stem-cell transplantation (HSCT) from his father. He was well and was not receiving intravenous immune globulin replacement therapy 13 months after undergoing HSCT.

In the first 2 years of life, Patient 2, a girl born to nonconsanguineous Finnish parents, had recurrent otitis media, pneumonia, diarrhea, and three episodes of thrombocytopenia that resolved spontaneously. At 2.5 years of age, vaccine strain–related varicella developed, with liver and lung involvement and multiple pulmonary infiltrates, and the patient required ventilatory support (Fig. 1B). Several months later, computed tomog-

The New England Journal of Medicine
Downloaded from nejm.org at Harvard Library on January 31, 2016. For personal use only. No other uses without permission.
Copyright © 2015 Massachusetts Medical Society. All rights reserved.

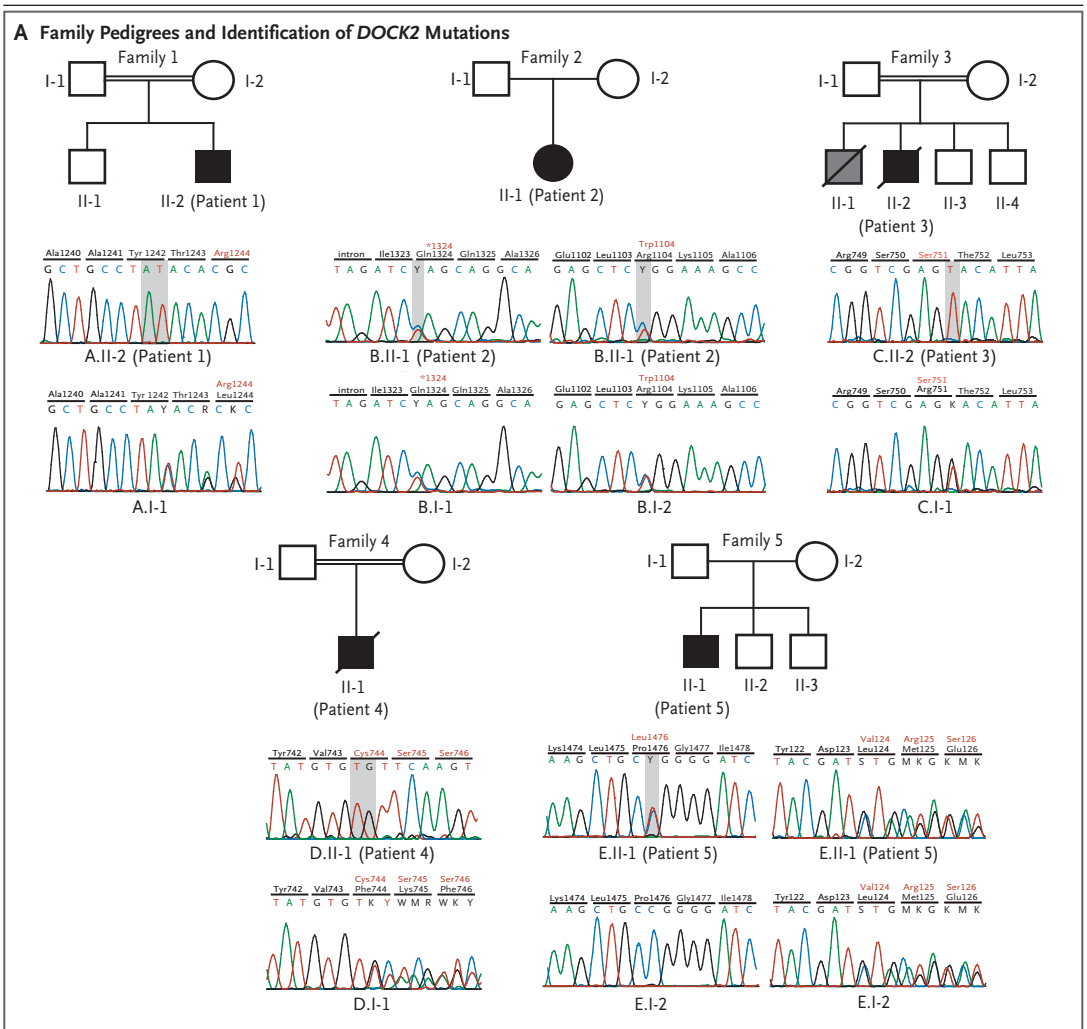

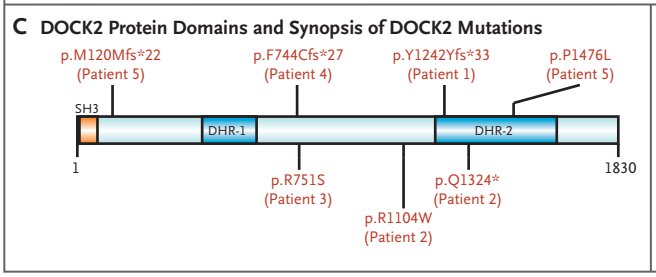

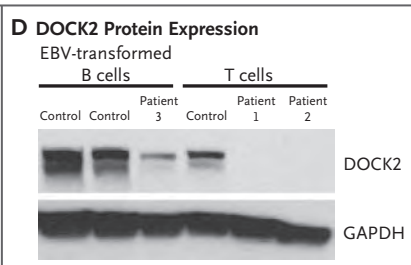

The New England Journal of Medicine
Downloaded from nejm.org at Harvard Library on January 31, 2016. For personal use only. No other uses without permission.
Copyright © 2015 Massachusetts Medical Society. All rights reserved.

Table 1. Immunologic Characteristics of Patients with DOCK2 Deficiency.*

Variable	Patient 1		Patient 2		Patient 3		Patient 4		Patient 5	
	Value	Reference Range	Value	Reference Range	Value	Reference Range	Value	Reference Range	Value	Reference Range
Age at evaluation	5 mo		2.5 yr		6.3 yr		1 yr		4 mo	
Absolute lymphocyte count (cells/mm^3 ×10^{-3})	1.22	3.9–9.0	1.24	2.3–5.4	1.1	1.9–3.7	2.3	3.6–8.9	4.4	3.9–9.0
Lymphocyte subset										
CD3+ T (cells/mm^3)	114	2500–5600	548	1400–3700	341	1200–2600	1173	2100–6200	830	2500–5600
CD4+ T (cells/mm^3)	57	1800–4000	305	700–2200	176	650–1500	129	1300–3400	511	1800–4000
CD45RA+CCR7+ (%)	4.0	76.7–91.4	0.4	65.2–84.8	NA		NA		4.5	76.7–91.4
CD45RA–CCR7+ (%)	16.0	6.7–15.6	19.2	10.5–23.2	NA		NA		33.8	6.7–15.6
CD45RA–CCR7– (%)	78.0	1.1–5.3	79.8	2.9–9.8	NA		NA		44.5	1.1–5.3
CD45RA+CCR7– (%)	12.0	0.1–1.9	0.6	0.2–3.0	NA		NA		17.2	0.1–1.9
CD8+ T (cells/mm^3)	24	590–1600	133	490–1300	187	370–1100	763	620–2000	319	590–1600
CD45RA+CCR7+ (%)	8.5	62.1–94.0	1.6	39.0–89.0	NA		NA		22	62.1–94.0
CD45RA–CCR7+ (%)	14.7	0.9–5.6	5.2	0.9–5.7	NA		NA		26.3	0.9–5.6
CD45RA–CCR7– (%)	72.1	1.3–19.5	74.0	3.4–28.2	NA		NA		9.8	1.3–19.5
CD45RA+CCR7– (%)	4.7	1.5–22.7	19.2	4.8–30.0	NA		NA		41.9	1.5–22.7
CD19+ B (cells/mm^3)	646	430–3000	146	390–1400	473	270–860	299	720–2600	1857	430–3000
CD3–CD56+/CD16+ (cells/mm^3)	191	170–830	489	130–720	187	100–480	138	180–920	1539	170–830
Immunoglobulin										
IgG (mg/dl)	350	172–814	788	424–1051	559	633–1280	821†	217–904	413	164–558
IgA (mg/dl)	77	8.1–84.0	422	14–123	131	33–202	192†	11–90	50	4.4–73.0
IgM (mg/dl)	24	33–108	37	48–168	82	48–207	31†	34–126	170	27–101
IgE (IU/ml)	NA		2704	0.3–29.5	41	1–161.3	5.28†	0.8–7.3	26†	0.4–3.8
Serum antibody responses	NA		Nonprotective against tetanus toxoid, PRP, *Streptococcus pneumoniae*		No response to VZV		Response to HBV not detectable		Response to KLH not detectable	

The New England Journal of Medicine
Downloaded from nejm.org at Harvard Library on January 31, 2016. For personal use only. No other uses without permission.
Copyright © 2015 Massachusetts Medical Society. All rights reserved.

TRECs at birth (copies/μl)	NA	<252‡	NA	<252‡	NA
T-cell response to phytohemagglutinin	2.6 (38.4)§	0.1 (278.2)§	9 (46–89)¶	18 (52–94)¶	6.04 (289.49)§

* Listed are reference ranges or laboratory values for the patient's age group. To convert values for IgE to micrograms per liter, multiply by 2.40. HBV denotes hepatitis B virus, KLH keyhole limpet hemocyanin, NA not assessed, PRP polyribosylribitol phosphate, TREC T-cell–receptor excision circle, and VZV varicella–zoster virus.

† This immunoglobulin level was measured when the patient was 9 months of age.

‡ The cutoff value for newborn screening for severe combined immunodeficiency in Massachusetts is shown. Normal amplification of the RNaseP reference gene was detected in dried blood spots obtained from both Patient 2 and Patient 4.

§ Stimulation index units (i.e., a response to phytohemagglutinin in counts per minute of radiolabeled thymidine incorporated minus counts per minute of background incorporation, divided by counts per minute of background incorporation) are shown. The T-cell response stimulation index units from a healthy control are shown in parentheses.

¶ The percentage of CD25+ cells after immunization with 10-valent pneumococcal protein-conjugate vaccine is shown. The range of the percentage of CD25+-expressing T cells in healthy controls is shown in parentheses.

raphy of the chest showed a new pulmonary infiltrate (Fig. S2A in the Supplementary Appendix). A lung biopsy revealed granulomatous inflammation (Fig. S2B in the Supplementary Appendix) with acid-fast bacilli. *Mycobacterium avium* was cultured from the biopsy specimen, and human herpesvirus-6 DNA was detected. Immunologic investigations revealed T-cell and B-cell lymphopenia, defective in vitro T-cell proliferation, and a lack of specific antibody responses (Table 1), all of which were consistent with combined immunodeficiency. At the age of 3.8 years, after reduced-intensity conditioning with the use of treosulfan, fludarabine, and alemtuzumab, she underwent HLA-matched unrelated-donor HSCT. She was well 8 months after HSCT.

Patient 3, a boy born to consanguineous Turkish parents, had recurrent respiratory tract infections from the age of 3 months. At 6 years of age, he had two episodes of meningoencephalitis. On the basis of examination of the cerebrospinal fluid (1000 leukocytes per cubic millimeter, 74% of which were lymphocytes), high serum amylase levels (762 U per liter), and detection of mumps-specific IgM, this condition was presumed to be due to mumps virus infection that was concurrent with an outbreak of mumps at the child's school. At the age of 6.3 years, severe varicella (Fig. 1B) with alveolar infiltrates developed, and child's illness rapidly progressed to multiorgan failure and death. Laboratory studies during the patient's hospitalization showed severe T-cell lymphopenia, impaired T-cell activation, and a lack of antibody responses to varicella–zoster virus (Table 1). A postmortem examination of the patient's liver and lungs revealed coagulation necrosis, apoptosis, inflammatory infiltrates with neutrophils and monocytes, and nuclear inclusion bodies within pneumocytes; the latter findings were consistent with viral pneumonitis (Fig. S2C and S2D in the Supplementary Appendix).

Patient 4, a boy born to consanguineous Turkish parents, had neonatal-onset chronic diarrhea with mucus and recurrent episodes of fever and oral moniliasis. A liver biopsy, performed at 3 months of age because of persistently elevated aminotransferase levels, revealed macrovesicular steatosis, nonnecrotic eosinophilic granuloma-like lesions, and lobular inflammation (Fig. S2E in the Supplementary Appendix). During hospital admission when the boy was 1 year of age,

The New England Journal of Medicine
Downloaded from nejm.org at Harvard Library on January 31, 2016. For personal use only. No other uses without permission.
Copyright © 2015 Massachusetts Medical Society. All rights reserved.

growth failure (body weight, 4.5 kg [3.5 kg below the 3rd percentile] and length, 64 cm [9 cm below the 3rd percentile]), a nodular erythematous lesion at the site of bacille Calmette–Guérin vaccination, and hepatomegaly were detected. In addition, histopathological analysis of the colon revealed focal active colitis (Fig. 1B) that was associated with a paucity of B cells, plasma cells, and to a lesser extent T cells in the lamina propria of the colon. Immunologic investigations (Table 1) revealed T-cell lymphopenia and defective T-cell activation in response to phytohemagglutinin. Subsequently, multiple episodes of pneumonia due to parainfluenza virus type 3 and adenovirus developed. The patient had several episodes of cytomegalovirus reactivation and died from *Klebsiella pneumoniae* sepsis at 20 months of age.

Patient 5, a Hispanic boy born to nonconsanguineous parents from Honduras and Nicaragua, presented at the age of 4 months with interstitial pneumonia that responded to high-dose trimethoprim–sulfamethoxazole. Immunologic findings were consistent with combined immunodeficiency (Table 1). At 2 years of age, a rectal fistula developed. At 3 years of age, he received an HSCT from his HLA-identical brother after conditioning with myeloablative doses of busulfan and cyclophosphamide. This patient was well and was not receiving intravenous immune globulin replacement therapy 17.5 years after transplantation.

Genetic, Immunologic, and Biochemical Analyses

Details of the methods for whole-exome sequencing, genomewide linkage analysis, homozygosity mapping, and sequencing analysis are provided in the Supplementary Appendix. In addition, the generation of T-cell, B-cell, and natural killer (NK)–cell lines are described in detail in the Supplementary Appendix, as are immunologic and biochemical studies of hematopoietic and nonhematopoietic cells.

Results

Immunologic Abnormalities

In all five patients, T-cell lymphopenia and impaired in vitro T-cell activation in response to phytohemagglutinin were detected (Table 1). Maternal T-cell engraftment was ruled out in all the patients. More detailed immunologic analyses that were performed in Patients 1, 2, and 5 revealed a markedly reduced proportion of naive (CD45RA+CCR7+) CD4+ and CD8+ T lymphocytes that were associated with an increased proportion of effector memory (CD45RA–CCR7–) CD4+ T lymphocytes and of either effector memory or CD45RA+CCR7– T_{EMRA} CD8+ T lymphocytes (Table 1). B-lymphocyte counts were reduced in Patients 2 and 4 (Table 1). Despite relatively normal serum levels of IgG and IgM, Patients 2, 4, and 5 had defective antibody production to T-cell–dependent immunization antigens (Table 1). Finally, in Patients 2 and 4, levels of T-cell–receptor excision circles, a marker of active thymopoiesis, were markedly reduced in dried blood spots obtained at birth (Table 1).

Identification of Biallelic Deleterious Mutations in *DOCK2*

Whole-exome sequencing was performed to elucidate the genetic basis of the patients' combined immunodeficiencies. Linkage analysis or homozygosity mapping were also performed in Patients 3 and 4, who were born to consanguineous parents. In Patients 1, 3, and 4, we selected genes harboring previously unreported homozygous variants, and in Patients 2 and 5 (for whom no parental consanguinity was known) we selected genes bearing two or more variants (Table S1 in the Supplementary Appendix). Biallelic mutations in *DOCK2* were identified and confirmed by means of Sanger sequencing in all five patients (Fig. 1A). No other gene harbored biallelic mutations in two or more patients. Patients 1 and 4 were homozygous for *DOCK2* dinucleotide insertions leading to frameshift and premature termination, Patient 3 was homozygous for a missense mutation, and Patients 2 and 5 were compound heterozygotes for different missense and nonsense *DOCK2* mutations (Fig. 1A). Multiple sequence alignment showed that all of the three missense mutations affect evolutionarily conserved residues (Fig. S3 in the Supplementary Appendix). Intrafamilial segregation was consistent with autosomal recessive inheritance with complete penetrance (Fig. S1 in the Supplementary Appendix). Collectively, we identified seven distinct rare mutations in *DOCK2* in five patients of various ethnic origins; four of these mutations led to premature termination, and three were predicted deleterious missense mutations affecting conserved residues of DOCK2 (Fig. 1C,

The New England Journal of Medicine
Downloaded from nejm.org at Harvard Library on January 31, 2016. For personal use only. No other uses without permission.
Copyright © 2015 Massachusetts Medical Society. All rights reserved.

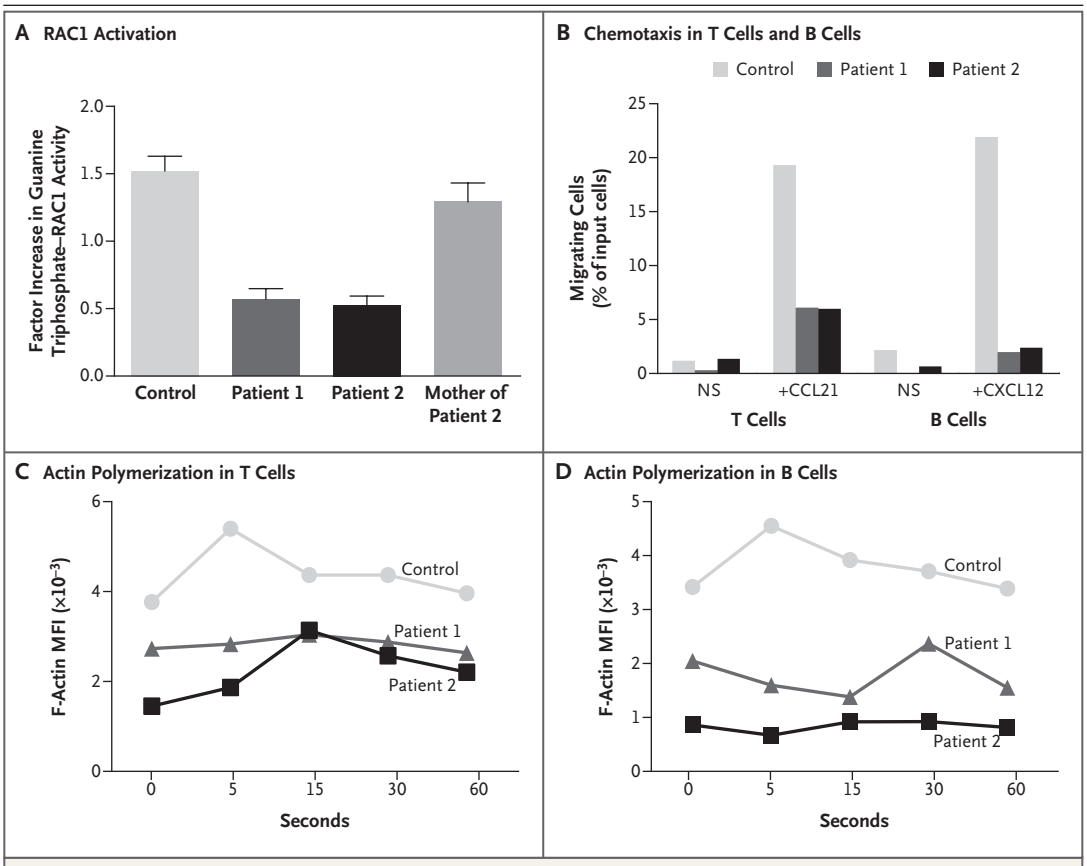

Figure 2. Defective RAC1 Activation, Lymphocyte Chemotaxis, and Actin Polymerization in Patients with DOCK2 Deficiency.

Panel A shows impaired RAC1 activation in T-cell lines from Patients 1 and 2 and Patient 2's mother (as compared with those from a healthy donor [control]), after stimulation of the T-cell receptor with the use of anti-CD3 monoclonal antibodies. One-way analysis of variance with Bonferroni correction was used to calculate the P values. T bars represent the standard-deviation values of three independent experiments. $P<0.001$ for all comparisons. Panel B shows reduced T-cell and B-cell migration in response to CCL21 or chemokine (C-X-C motif) ligand 12 (CXCL12) in Patients 1 and 2 as compared with a healthy control. NS denotes not stimulated. Panels C and D show reduced levels of polymerized, filamentous actin (F-actin) in Patients 1 and 2, as revealed by phalloidin staining in T cells (Panel C) and B cells (Panel D). MFI denotes mean fluorescence intensity.

and Table S2 and Fig. S3 in the Supplementary Appendix).

Effect of *DOCK2* Mutations on Protein Expression and T-Cell and B-Cell Signaling

Immunoblot analysis revealed no DOCK2 protein expression in T-cell lines obtained from Patient 1 and trace amounts in Patient 2; markedly reduced levels of protein were detected in Epstein–Barr virus–transformed B cells obtained from Patient 3 (Fig. 1D, and Fig. S4A in the Supplementary Appendix). No biologic specimens from Patients 4 and 5 were available; however, overexpression of streptavidin–hemagglutinin–tagged DOCK2 bearing the p.F744Cfs*27 mutation (present in Patient 4) showed expression of a truncated DOCK2 protein (Fig. S4B in the Supplementary Appendix) that lacks the DOCK homology region 2 domain that is critical for the DOCK2 guanine nucleotide exchange factor function.

Previous studies involving mice have shown that Dock2 is essential for Rac1 activation downstream of the T-cell receptor.[8,9] In our study, after activation of polyclonal human T-cell lines with an anti-CD3 monoclonal antibody, guanine triphosphate–bound RAC1 was clearly detected in T cells from a healthy control and from Patient 2's

The New England Journal of Medicine
Downloaded from nejm.org at Harvard Library on January 31, 2016. For personal use only. No other uses without permission.
Copyright © 2015 Massachusetts Medical Society. All rights reserved.

mother, but not from Patients 1 and 2 (Fig. 2A, and Fig. S5 in the Supplementary Appendix).

Chemokine-mediated cell migration is critically important during lymphocyte development, immune surveillance of lymph nodes, and recruitment of immune cells to sites of inflammation. Previous experimental data suggested a role for DOCK2 in actin polymerization and chemotactic responses of T lymphocytes and B lymphocytes after chemokine stimulation.[9,10] Indeed, the chemotactic response of T cells and B cells obtained from Patients 1 and 2 was profoundly impaired (Fig. 2B). Furthermore, chemokine (C-X-C motif) ligand 12 (CXCL12)–induced actin polymerization in T cells and B cells from Patients 1 and 2 was impaired and delayed (Fig. 2C and 2D). Baseline levels of polymerized actin (filamentous actin [F-actin]) were also reduced in DOCK2-deficient T lymphocytes and B lymphocytes from Patients 1 and 2 (Fig. 2C and 2D).

DEFECTS IN NK CELLS AND NK T CELLS IN PATIENTS WITH DOCK2 DEFICIENCY

Invasive viral infections were a prominent clinical feature in Patients 2, 3, and 4. Patients with DOCK2 deficiency had normal numbers of CD3–CD56+/CD16+ NK cells (Table 1), and NK cells from Patient 2 had a normal immunophenotype (Fig. S6 in the Supplementary Appendix). However, NK cells from Patients 1 and 2 showed impaired degranulation after stimulation with the human erythroleukemia cell line K562 (Fig. 3A).

The ability of NK cells to lyse virus-infected and tumor-target cells correlates with the functionality of a variety of activating NK receptors interacting with distinct adaptor (DAP10 and DAP12) and signaling (CD3ζ, FcεRIγ) molecules.[11-13] The triggering of activating NK receptors induces actin polymerization, activation of phosphatidylinositol-3-OH kinase, and phosphorylation of extracellular signal-regulated kinase (ERK) and mitogen-activated protein–ERK (MEK), ultimately promoting NK-cell cytotoxicity.[14]

We analyzed NK-cell degranulation after engagement of CD16, NKp30 (NK-cell p30-related protein), or NKp46 (NK-cell p46-related protein) — all of which use CD3ζ and FcεRIγ — or NKG2D (which recruits the DAP10 adaptor). We observed severely impaired degranulation in Patient 1 (Fig. 3B) and moderately impaired degranulation in Patient 2, probably corresponding to residual amounts of DOCK2 protein in Patient 2's hematopoietic cells (Fig. S4A in the Supplementary Appendix). Degranulation was also impaired in Patient 2's interleukin-2–activated polyclonal NK cells after engagement of NKp44 (NK-cell p44-related protein) (which uses DAP12) (Fig. S7 in the Supplementary Appendix). Furthermore, we observed reduced levels of F-actin in Patient 2's NK cells after stimulation with anti-CD16 and anti-NKp46 monoclonal antibodies (Fig. 3C); these findings were reminiscent of observations in *Dock2*$^{-/-}$ mice.[15] These reduced levels possibly reflected impaired tonal signaling through antigen and chemokine receptors. Reduced phosphorylation of ERK1/2 and MEK and impaired actin polymerization were also detected in polyclonal NK cells from Patient 2 after cross-linking of NKp30, NKp44 (Fig. 3D), CD16, and NKp46. NK cells are also involved in cytokine production.[16] After overnight stimulation with interleukin-12 and interleukin-18, the proportion of NK cells expressing interferon-γ was markedly reduced in Patient 2 (Fig. 3E).

Finally, the number of circulating NK T cells was severely reduced in Patients 1 and 2 (Fig. S8 in the Supplementary Appendix). Altogether, these data show that DOCK2 serves an essential role in NK and NK T-cell biology; these findings are consistent with similar observations in mice.[17,18]

IMPAIRED ANTIVIRAL INTERFERON RESPONSES IN PATIENTS WITH DOCK2 DEFICIENCY

Human interferon-α/β and interferon-λ immunity has been suggested to be essential in host defense against viral infections.[19] Plasmacytoid dendritic cells are the major source of interferon-α in human blood in response to enveloped viruses and synthetic toll-like receptor 7 and toll-like receptor 9 agonists.[20] Previous studies involving mice have shown that Dock2 serves an essential function in regulating interferon-α production in plasmacytoid dendritic cells without perturbing development of these cells.[15,21]

Although a normal proportion of circulating plasmacytoid dendritic cells was detected in Patient 2 (Fig. S9 in the Supplementary Appendix), the production of interferon-α and interferon-λ in the peripheral-blood mononuclear cells (PBMCs) in Patients 1, 2, and 3 after stimulation with herpes simplex virus type 1 (HSV-1) or vesicular stomatitis virus (VSV) was markedly impaired (Fig. 4A, and Fig. S10 in the Supplementary Appendix). By contrast, similar amounts of inter-

The New England Journal of Medicine
Downloaded from nejm.org at Harvard Library on January 31, 2016. For personal use only. No other uses without permission.
Copyright © 2015 Massachusetts Medical Society. All rights reserved.

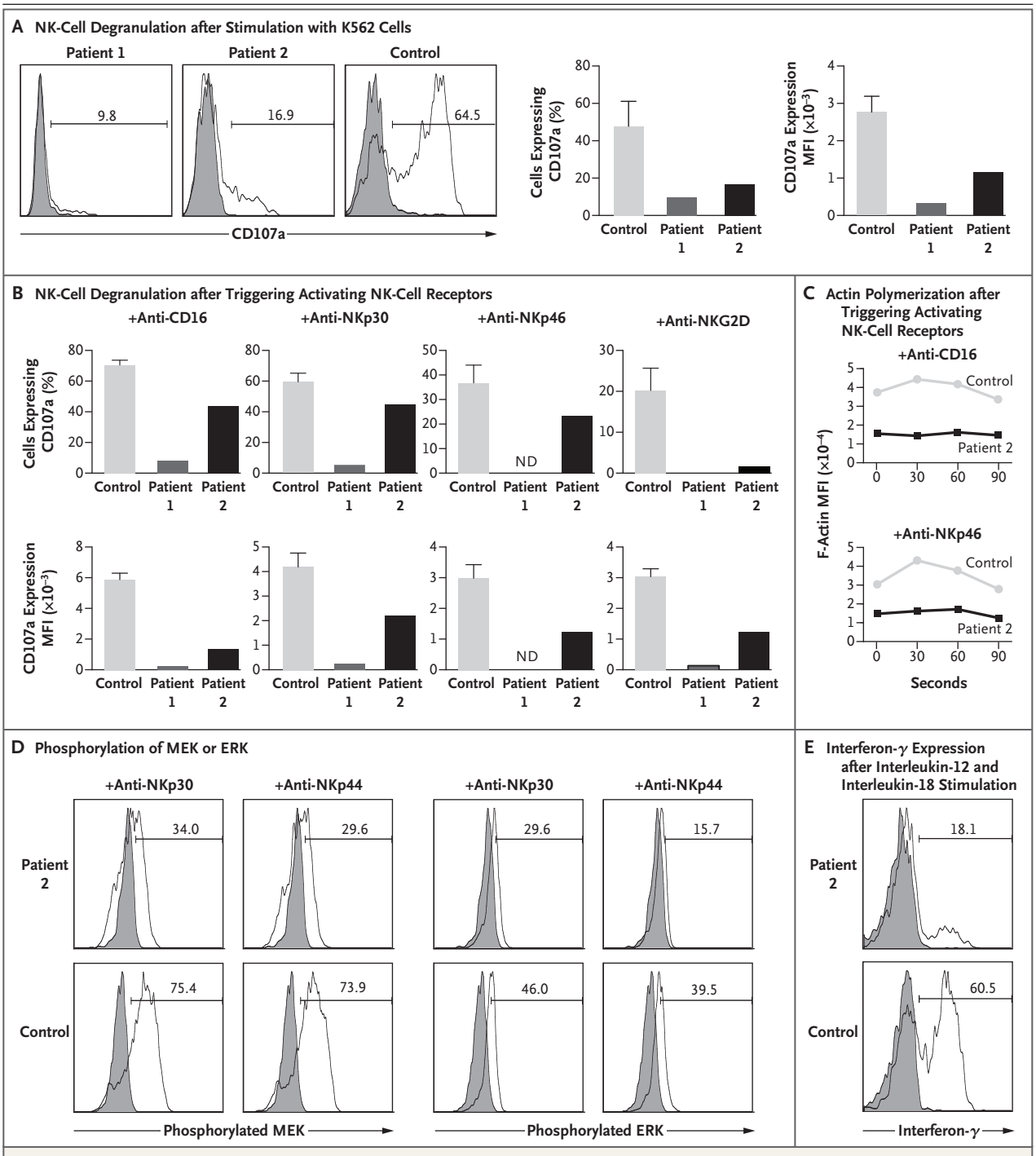

Figure 3. NK-Cell Cytotoxicity and Signaling Defects in Patients with DOCK2 Deficiency.

Panel A shows impaired NK-cell degranulation (as measured by CD107a surface expression) after stimulation with K562 cells in Patients 1 and 2, as compared with 10 healthy controls. Horizontal bars represent means, and T bars means ±SD. Panel B shows defective degranulation after triggering of activating NK-cell receptors in Patients 1 and 2, as compared with 6 healthy controls. Horizontal bars represent means, and T bars means ±SD. ND denotes not done. Panel C shows impaired actin polymerization after triggering of activating NK-cell receptors CD16 (top) and NKp46 (bottom). Panel D shows impaired extracellular signal-regulated kinase (ERK) and mitogen-activated protein–ERK (MEK) phosphorylation in NK cells from Patient 2 after triggering of activating receptors, as detected by means of flow cytometry. Panel E shows decreased interferon-γ production after NK-cell stimulation with interleukin-12 and interleukin-18 in Patient 2, as compared with a healthy control.

The New England Journal of Medicine
Downloaded from nejm.org at Harvard Library on January 31, 2016. For personal use only. No other uses without permission.
Copyright © 2015 Massachusetts Medical Society. All rights reserved.

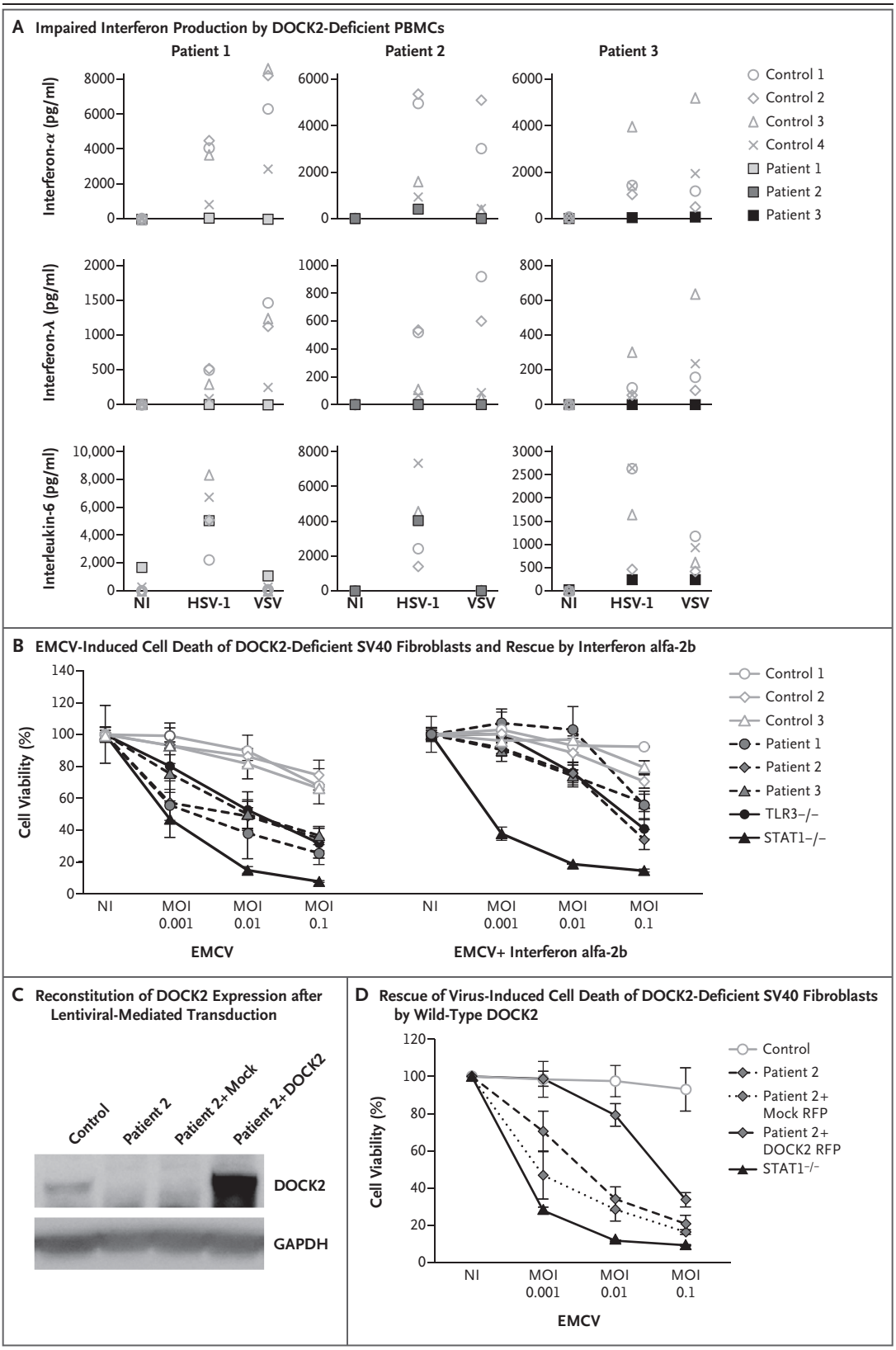

The New England Journal of Medicine
Downloaded from nejm.org at Harvard Library on January 31, 2016. For personal use only. No other uses without permission.
Copyright © 2015 Massachusetts Medical Society. All rights reserved.

Figure 4 (facing page). Impaired Interferon Responses to Viruses in DOCK2-Deficient Leukocytes and Fibroblasts.

Panel A shows impaired interferon-α and interferon-λ production by DOCK2-deficient peripheral-blood mononuclear cells (PBMCs) after exposure to either herpes simplex virus 1 (HSV-1) or vesicular stomatitis virus (VSV) for 24 hours each. By contrast, production of interleukin-6 by the patients' PBMCs was similar to that in the PBMCs of the healthy donors (controls) and served as an assay control. NI denotes not infected. Panel B shows increased encephalomyocarditis virus (EMCV)–induced cell death of DOCK2-deficient simian virus 40 (SV40) fibroblasts (left) and rescue by the addition of interferon alfa-2b (right). Toll-like receptor 3 (TLR3)–deficient and signal transducer and activator of transcription 1 (STAT1)–deficient SV40 fibroblast cell lines served as examples of defective interferon-dependent antiviral immunity. I bars represent the standard-deviation values of triplicate measurements from one representative experiment of three experiments performed. MOI denotes multiplicity of infection. Panel C shows immunoblot analysis of protein lysates obtained from SV40 fibroblasts from a healthy donor (control) and Patient 2, as well as from mock-transduced (Mock) and DOCK2-transduced fibroblasts from Patient 2. Panel D shows rescue of EMCV-induced cell death of SV40 fibroblasts from Patient 2 by exogenous expression of wild-type *DOCK2*. STAT1-deficient fibroblasts were used as a negative control. The data in Panels B and D show one representative experiment of three independent experiments with technical triplicates carried out in each experiment.

leukin-6 were produced by PBMCs in samples obtained from patients with DOCK2 deficiency and from healthy donors (Fig. 4A, and Fig. S10 in the Supplementary Appendix). Altogether, these data indicate that in addition to T cells, NK cells, and NK T cells, plasmacytoid dendritic cells may also be defective in patients with DOCK2 deficiency; this may also contribute to the patients' viral susceptibility.

Although DOCK2 is preferentially expressed in hematopoietic cells,[22] low levels of expression were detected in fibroblasts from healthy controls, but not from Patients 1 and 2 (Fig. S4A in the Supplementary Appendix). Only minimal expression was detected in fibroblasts from Patient 3 (Fig. S4A in the Supplementary Appendix). To investigate whether DOCK2 contributes to cell-intrinsic antiviral responses in nonhematopoietic tissues, we studied simian virus 40 (SV40)–immortalized fibroblasts from Patients 1, 2, and 3 and from healthy controls. After infection with VSV or encephalomyocarditis virus, we found enhanced levels of viral replication and decreased viability of DOCK2-deficient SV40 fibroblasts (Fig. 4B, and Fig. S11 in the Supplementary Appendix); similar results were observed in SV40 fibroblasts from patients with toll-like receptor 3 or signal transducer and activator of transcription 1 deficiency (Fig. 4B, and Fig. S11 in the Supplementary Appendix), which affect the production of or the response to interferon-α/β and interferon-λ, respectively.[23]

Both treatment with recombinant interferon alfa-2b (Fig. 4B) and lentiviral-mediated wild-type DOCK2 expression (Fig. 4C) protected DOCK2-deficient fibroblasts from virus-induced cell death (Fig. 4D). The *DOCK2* mutations may therefore also impair cell-intrinsic, nonhematopoietic immunity, at least in fibroblasts and in response to some viruses.

DISCUSSION

In this study, we showed that biallelic mutations in *DOCK2* were the molecular cause of a distinctive type of combined immunodeficiency that is characterized by early-onset, invasive bacterial and viral infections; T-cell lymphopenia; impaired T-cell, B-cell, and NK-cell function; and defective interferon immunity in both hematopoietic and nonhematopoietic cells. Our results also indicate that this disease can be detected at birth with newborn screening for severe combined immunodeficiency (Table 1) and can be cured by means of HSCT (Fig. S12 in the Supplementary Appendix).

The observation that DOCK2 deficiency in humans leads to impaired RAC1 activation and to defects in actin polymerization, T-cell proliferation, chemokine-induced lymphocyte migration, and NK-cell degranulation confirms and extends similar observations in *Dock2*$^{-/-}$ mice.[9,10,17,24] It also highlights the essential role of regulated actin dynamics for immune-cell function, a role that is also evident with respect to other combined immunodeficiencies involving defective actin polymerization such as the Wiskott–Aldrich syndrome,[25] as well as with respect to deficiency of Wiskott–Aldrich syndrome protein–interacting protein (WIP),[26] DOCK8 protein,[27] the protein encoded by the Ras homologue family member H (RHOH),[28] and macrophage-stimulating 1 growth factor (MST1) protein.[29,30]

The occurrence of invasive viral infections, including disseminated vaccine-strain varicella,

The New England Journal of Medicine
Downloaded from nejm.org at Harvard Library on January 31, 2016. For personal use only. No other uses without permission.
Copyright © 2015 Massachusetts Medical Society. All rights reserved.

was a prominent feature in patients with DOCK2 deficiency. Human antiviral immunity is critically dependent on intact T-cell function as well as on innate immune responses, as observed in patients with genetic defects affecting T-cell, NK-cell, NK T-cell, and dendritic-cell development, function, or both,[1,31] or with mutations affecting production of (or response to) interferon-α, interferon-β, and interferon-λ in both hematopoietic and nonhematopoietic cells.[32] We observed defective interferon-α/β and interferon-λ responses in both hematopoietic and nonhematopoietic cells in patients with DOCK2 deficiency. Plasmacytoid dendritic cells are the most potent interferon-α–producing cells.[33] Severe reduction of splenic and lymph-node plasmacytoid dendritic cells and of their capability for interferon-α production were observed in *Dock2*$^{-/-}$ mice.[15,21] Here we show impaired interferon-α and interferon-λ production in DOCK2-deficient PBMCs after stimulation with HSV-1 or VSV, possibly reflecting a defect of plasmacytoid dendritic cells. Therefore, we speculate that treatment with interferon alfa-2b might be beneficial in patients with DOCK2 deficiency who have severe viral infections.

Furthermore, our study suggests a role for DOCK2 in antiviral responses in nonhematopoietic cells. DOCK2 deficiency in nonhematopoietic cells may contribute to the pathogenesis of severe viral infections. Normalization of immunologic abnormalities and resolution of infections were observed in Patients 1, 2, and 5 after HSCT (Fig. S12 in the Supplementary Appendix). This finding implies that correction of hematopoietic cells may be sufficient to rescue the clinical phenotype, possibly by providing a source of cells producing interferon-α/β (e.g., plasmacytoid dendritic cells) and therefore complementing the defect in nonhematopoietic tissues.

K. pneumoniae sepsis was the cause of death in Patient 4. Susceptibility to invasive bacterial infections in patients with DOCK2 deficiency may reflect impaired function of neutrophil granulocytes in addition to impaired antibody production. Defective neutrophil chemotaxis has been reported in *Dock2*$^{-/-}$ mice.[34] Because of a lack of primary material, we could not test whether a similar defect existed in the patients in our study.

Mutations in *DOCK8*, another member of the DOCK family of proteins, have been identified in patients with another form of combined immunodeficiency.[35,36] Similarities and important differences have been observed between patients with DOCK2 deficiency and those with DOCK8 deficiency. Both conditions are characterized by recurrent bacterial and viral infections[36] and are associated with T-cell lymphopenia,[36] defective NK-cell function,[37] aberrant NK T-cell survival and function,[38] and impaired antibody responses.[39] However, the natural course of DOCK2 deficiency appears to be more severe than that of DOCK8 deficiency. Although DOCK8 deficiency is characterized mostly by cutaneous viral infections,[36] patients with DOCK2 deficiency have early-onset, life-threatening, invasive viral and bacterial infections. Furthermore, severe food allergies, eczema, and autoimmunity are commonly observed in patients with DOCK8 deficiency,[36,40,41] whereas none of the patients with DOCK2 deficiency had such manifestations.

In summary, we have identified DOCK2 deficiency as a pleiotropic immunodeficiency leading to early-onset, invasive bacterial and viral infections. The broad spectrum of infections observed in patients with DOCK2 deficiency highlights the effect of DOCK2 function on several aspects of immunity and arouses possible concern about the application of new immunosuppressive agents targeting DOCK2.[42] Our observations indicate that HSCT can provide a cure for this immunodeficiency.

Supported by grants from the National Institutes of Health (5R01AI100887-03, to Dr. Notarangelo), the Manton Foundation (to Dr. Notarangelo), the European Research Council (ERC starting grant 310857, to Dr. Boztuğ), the Austrian Science Fund START program (Y595-B13, to Dr. Boztuğ), the National Center for Research Resources and the National Center for Advancing Translational Sciences (8 UL1TR000043, to Dr. Casanova), the German Research Foundation (for the Cluster of Excellence REBIRTH EXC 62/1 and CRC738, to Dr. Schambach), the New England Newborn Screening Program, University of Massachusetts Medical School (to Dr. Comeau), the Scientific and Technological Research Council of Turkey (1059B191300622, to Dr. Keles), Union Chimique Belge Celltech (to Dr. Goldstein), and Baxter Healthcare (to Dr. Buckley).

Disclosure forms provided by the authors are available with the full text of this article at NEJM.org.

We thank the patients and families for their support of the study; Drs. Katharina Willmann, Elisabeth Salzer, Marija Zore, Tatjana Hirschmugl, Minji Byun, Avinash Abhyankar, Dusan Bogunovic, Melina Herman, Xiao-Fei Kong, Lazaro Lorenzo, Sophie Cypowyj, Olivier Manches, Emmanuelle Jouanguy, Kenneth Cronin, and Mary-Ellen Conley for help with experimental procedures and discussions; and the Exome Aggregation Consortium (ExAC) and the groups that provided exome variant data for comparison. A full list of the ExAC contributing projects is provided at http://exac.broadinstitute.org/about.

The New England Journal of Medicine
Downloaded from nejm.org at Harvard Library on January 31, 2016. For personal use only. No other uses without permission.
Copyright © 2015 Massachusetts Medical Society. All rights reserved.

APPENDIX

The authors' full names and academic degrees are as follows: Kerry Dobbs, B.S., Cecilia Domínguez Conde, M.Sc., Shen-Ying Zhang, M.D., Ph.D., Silvia Parolini, Ph.D., Magali Audry, Ph.D., Janet Chou, M.D., Emma Haapaniemi, M.D., Sevgi Keles, M.D., Ivan Bilic, Ph.D., Satoshi Okada, M.D., Ph.D., Michel J. Massaad, Ph.D., Samuli Rounioja, M.D., Ph.D., Adel M. Alwahadneh, M.D., Nina K. Serwas, M.Sc., Kelly Capuder, B.S., Ergin Çiftçi, M.D., Kerstin Felgentreff, M.D., Toshiro K. Ohsumi, Ph.D., Vincent Pedergnana, Ph.D., Bertrand Boisson, Ph.D., Şule Haskologlu, M.D., Arzu Ensari, M.D., Ph.D., Michael Schuster, Ph.D., Alessandro Moretta, M.D., Yuval Itan, Ph.D., Ornella Patrizi, Ph.D., Flore Rozenberg, M.D., Pierre Lebon, M.D., Janna Saarela, M.D., Ph.D., Mikael Knip, M.D., Ph.D., Slavé Petrovski, Ph.D., David B. Goldstein, Ph.D., Roberta E. Parrott, B.S., Berna Savas, M.D., Ph.D., Axel Schambach, M.D., Ph.D., Giovanna Tabellini, Ph.D., Christoph Bock, Ph.D., Talal A. Chatila, M.D., Anne Marie Comeau, Ph.D., Raif S. Geha, M.D., Laurent Abel, M.D., Ph.D., Rebecca H. Buckley, M.D., Aydan İkincioğulları, M.D., Waleed Al-Herz, M.D., Merja Helminen, M.D., Ph.D., Figen Doğu, M.D., Jean-Laurent Casanova, M.D., Ph.D., Kaan Boztuğ, M.D., and Luigi D. Notarangelo, M.D.

The authors' affiliations are as follows: the Division of Immunology (K.D., J.C., S.K., M.J.M., K.C., K.F., T.A.C., R.S.G., L.D.N.) and Manton Center for Orphan Disease Research (L.D.N.), Boston Children's Hospital, and Department of Molecular Biology, Massachusetts General Hospital (T.K.O.), Boston, Harvard Stem Cell Institute, Harvard University, Cambridge (L.D.N.), and Department of Pediatrics, University of Massachusetts Medical School, Worcester (A.M.C.) — all in Massachusetts; CeMM Research Center for Molecular Medicine of the Austrian Academy of Sciences (C.D.C., I.B., N.K.S., M.S., C.B., K.B.), Department of Pediatrics and Adolescent Medicine, Medical University of Vienna (K.B.), and CeRUD Vienna Center for Rare and Undiagnosed Diseases (K.B.) — all in Vienna; St. Giles Laboratory of Human Genetics of Infectious Disease, Rockefeller Branch, Rockefeller University (S.-Y.Z., M.A., S.O., B.B., Y.I., L.A., J.-L.C.), and Institute for Genomic Medicine, Columbia University (S. Petrovski, D.B.G.) — both in New York; Laboratory of Human Genetics of Infectious Diseases, Necker Branch, INSERM Unité 1163 (S.-Y.Z., V.P., L.A., J.-L.C.), Paris Descartes University, Sorbonne Paris Cité, Imagine Institute (S.-Y.Z., F.R., P.L., L.A., J.-L.C.), and Pediatric Hematology-Immunology Unit, Necker Hospital for Sick Children (J.-L.C.) — all in Paris; Howard Hughes Medical Institute, Chevy Chase, MD (J.-L.C.); Department of Molecular and Translational Medicine, University of Brescia, Brescia (S. Parolini, O.P., G.T.), and Department of Experimental Medicine and Center of Excellence for Biomedical Research, University of Genoa, Genoa (A.M.) — both in Italy; Folkhälsan Institute of Genetics and Research Programs Unit, Molecular Neurology (E.H.), Institute for Molecular Medicine Finland (J.S.), Children's Hospital (M.K.), Research Programs Unit, Diabetes and Obesity Research Program (M.K.), and Folkhälsan Research Center (M.K.), University of Helsinki and Helsinki University Central Hospital, Helsinki, Tampere Center for Child Health Research (S.R., M.K., M.H.), and Fimlab Laboratories (S.R.), Tampere University Hospital, Tampere — all in Finland; Division of Pediatric Immunology and Allergy, Meram Faculty of Medicine, Necmettin Erbakan University, Konya (S.K.), and Departments of Pediatric Infectious Disease (E.Ç.), Immunology and Allergy (Ş.H., A.İ., F.D.), and Pathology (A.E., B.S.), Ankara University Medical School, Ankara — all in Turkey; Pediatric Allergy, Immunology, and Rheumatology Section, Queen Rania Pediatric Hospital, King Hussein Medical Center, Amman, Jordan (A.M.A.); Institute of Experimental Hematology, Hannover Medical School, Hannover, Germany (A.S.); Duke Center for Human Genome Variation (S. Petrovski, D.B.G.), Division of Allergy and Immunology, Department of Pediatrics (R.E.P., R.H.B.), and Department of Immunology (R.H.B.), Duke University School of Medicine — all in Durham, NC; and Department of Pediatrics, Faculty of Medicine, Kuwait University, Safat, Kuwait (W.A.-H.).

REFERENCES

1. Al-Herz W, Bousfiha A, Casanova JL, et al. Primary immunodeficiency diseases: an update on the classification from the International Union of Immunological Societies expert committee for primary immunodeficiency. Front Immunol 2014; 5:162.
2. Notarangelo LD. Functional T cell immunodeficiencies (with T cells present). Annu Rev Immunol 2013;31:195-225.
3. Koboldt DC, Steinberg KM, Larson DE, Wilson RK, Mardis ER. The next-generation sequencing revolution and its impact on genomics. Cell 2013;155:27-38.
4. Conley ME, Casanova JL. Discovery of single-gene inborn errors of immunity by next generation sequencing. Curr Opin Immunol 2014;30:17-23.
5. Ng SB, Buckingham KJ, Lee C, et al. Exome sequencing identifies the cause of a mendelian disorder. Nat Genet 2010;42: 30-5.
6. Yang Y, Muzny DM, Reid JG, et al. Clinical whole-exome sequencing for the diagnosis of mendelian disorders. N Engl J Med 2013;369:1502-11.
7. Casanova JL, Conley ME, Seligman SJ, Abel L, Notarangelo LD. Guidelines for genetic studies in single patients: lessons from primary immunodeficiencies. J Exp Med 2014;211:2137-49.
8. Sanui T, Inayoshi A, Noda M, et al. DOCK2 regulates Rac activation and cytoskeletal reorganization through interaction with ELMO1. Blood 2003;102:2948-50.
9. Fukui Y, Hashimoto O, Sanui T, et al. Haematopoietic cell-specific CDM family protein DOCK2 is essential for lymphocyte migration. Nature 2001;412:826-31.
10. Nombela-Arrieta C, Lacalle RA, Montoya MC, et al. Differential requirements for DOCK2 and phosphoinositide-3-kinase gamma during T and B lymphocyte homing. Immunity 2004;21:429-41.
11. Biassoni R. Human natural killer receptors, co-receptors, and their ligands. Curr Protoc Immunol 2009;Chapter 14: Unit 14.10.
12. Montaldo E, Del Zotto G, Della Chiesa M, et al. Human NK cell receptors/markers: a tool to analyze NK cell development, subsets and function. Cytometry A 2013; 83:702-13.
13. Tassi I, Klesney-Tait J, Colonna M. Dissecting natural killer cell activation pathways through analysis of genetic mutations in human and mouse. Immunol Rev 2006;214:92-105.
14. Rajasekaran K, Kumar P, Schuldt KM, et al. Signaling by Fyn-ADAP via the Carma1-Bcl-10-MAP3K7 signalosome exclusively regulates inflammatory cytokine production in NK cells. Nat Immunol 2013;14:1127-36.
15. Gotoh K, Tanaka Y, Nishikimi A, et al. Differential requirement for DOCK2 in migration of plasmacytoid dendritic cells versus myeloid dendritic cells. Blood 2008; 111:2973-6.
16. Vivier E, Tomasello E, Baratin M, Walzer T, Ugolini S. Functions of natural killer cells. Nat Immunol 2008;9:503-10.
17. Sakai Y, Tanaka Y, Yanagihara T, et al. The Rac activator DOCK2 regulates natural killer cell-mediated cytotoxicity in mice through the lytic synapse formation. Blood 2013;122:386-93.
18. Kunisaki Y, Tanaka Y, Sanui T, et al. DOCK2 is required in T cell precursors for development of Valpha14 NK T cells. J Immunol 2006;176:4640-5.
19. Zhang SY, Boisson-Dupuis S, Chapgier A, et al. Inborn errors of interferon (IFN)-mediated immunity in humans: insights into the respective roles of IFN-alpha/beta, IFN-gamma, and IFN-lambda in host defense. Immunol Rev 2008;226: 29-40.
20. Swiecki M, Colonna M. Unraveling the functions of plasmacytoid dendritic cells during viral infections, autoimmunity, and tolerance. Immunol Rev 2010; 234:142-62.

The New England Journal of Medicine
Downloaded from nejm.org at Harvard Library on January 31, 2016. For personal use only. No other uses without permission.
Copyright © 2015 Massachusetts Medical Society. All rights reserved.

21. Gotoh K, Tanaka Y, Nishikimi A, et al. Selective control of type I IFN induction by the Rac activator DOCK2 during TLR-mediated plasmacytoid dendritic cell activation. J Exp Med 2010;207:721-30.
22. Nishihara H, Kobayashi S, Hashimoto Y, et al. Non-adherent cell-specific expression of DOCK2, a member of the human CDM-family proteins. Biochim Biophys Acta 1999;1452:179-87.
23. Zhang SY, Herman M, Ciancanelli MJ, et al. TLR3 immunity to infection in mice and humans. Curr Opin Immunol 2013; 25:19-33.
24. Sanui T, Inayoshi A, Noda M, et al. DOCK2 is essential for antigen-induced translocation of TCR and lipid rafts, but not PKC-theta and LFA-1, in T cells. Immunity 2003;19:119-29.
25. Thrasher AJ, Burns SO. WASP: a key immunological multitasker. Nat Rev Immunol 2010;10:182-92.
26. Lanzi G, Moratto D, Vairo D, et al. A novel primary human immunodeficiency due to deficiency in the WASP-interacting protein WIP. J Exp Med 2012;209:29-34.
27. McGhee SA, Chatila TA. DOCK8 immune deficiency as a model for primary cytoskeletal dysfunction. Dis Markers 2010;29:151-6.
28. Crequer A, Troeger A, Patin E, et al. Human RHOH deficiency causes T cell defects and susceptibility to EV-HPV infections. J Clin Invest 2012;122:3239-47.
29. Abdollahpour H, Appaswamy G, Kotlarz D, et al. The phenotype of human STK4 deficiency. Blood 2012;119:3450-7.
30. Nehme NT, Pachlopnik Schmid J, Debeurme F, et al. MST1 mutations in autosomal recessive primary immunodeficiency characterized by defective naive T-cell survival. Blood 2012;119:3458-68.
31. Fischer A. Human primary immunodeficiency diseases. Immunity 2007;27: 835-45.
32. Casanova JL, Abel L, Quintana-Murci L. Immunology taught by human genetics. Cold Spring Harb Symp Quant Biol 2013; 78:157-72.
33. Colonna M, Trinchieri G, Liu YJ. Plasmacytoid dendritic cells in immunity. Nat Immunol 2004;5:1219-26.
34. Nishikimi A, Fukuhara H, Su W, et al. Sequential regulation of DOCK2 dynamics by two phospholipids during neutrophil chemotaxis. Science 2009;324:384-7.
35. Engelhardt KR, McGhee S, Winkler S, et al. Large deletions and point mutations involving the dedicator of cytokinesis 8 (DOCK8) in the autosomal-recessive form of hyper-IgE syndrome. J Allergy Clin Immunol 2009;124(6):1289.e4-1302.e4.
36. Zhang Q, Davis JC, Lamborn IT, et al. Combined immunodeficiency associated with DOCK8 mutations. N Engl J Med 2009;361:2046-55.
37. Mizesko MC, Banerjee PP, Monaco-Shawver L, et al. Defective actin accumulation impairs human natural killer cell function in patients with dedicator of cytokinesis 8 deficiency. J Allergy Clin Immunol 2013;131:840-8.
38. Crawford G, Enders A, Gileadi U, et al. DOCK8 is critical for the survival and function of NKT cells. Blood 2013;122: 2052-61.
39. Jabara HH, McDonald DR, Janssen E, et al. DOCK8 functions as an adaptor that links TLR-MyD88 signaling to B cell activation. Nat Immunol 2012;13:612-20.
40. Janssen E, Tsitsikov E, Al-Herz W, et al. Flow cytometry biomarkers distinguish DOCK8 deficiency from severe atopic dermatitis. Clin Immunol 2014;150:220-4.
41. Janssen E, Morbach H, Ullas S, et al. Dedicator of cytokinesis 8-deficient patients have a breakdown in peripheral B-cell tolerance and defective regulatory T cells. J Allergy Clin Immunol 2014;134: 1365-74.
42. Nishikimi A, Uruno T, Duan X, et al. Blockade of inflammatory responses by a small-molecule inhibitor of the Rac activator DOCK2. Chem Biol 2012;19:488-97.

Copyright © 2015 Massachusetts Medical Society.

RECEIVE IMMEDIATE NOTIFICATION WHEN AN ARTICLE IS PUBLISHED ONLINE FIRST

To be notified by e-mail when *Journal* articles are published Online First, sign up at NEJM.org.

The New England Journal of Medicine
Downloaded from nejm.org at Harvard Library on January 31, 2016. For personal use only. No other uses without permission.
Copyright © 2015 Massachusetts Medical Society. All rights reserved.

Supplementary Appendix

This appendix has been provided by the authors to give readers additional information about their work.

Supplement to: Dobbs K, Domínguez Conde C, Zhang S-Y, et al. Inherited DOCK2 deficiency in patients with early-onset invasive infections. N Engl J Med 2015;372:2409-22. DOI: 10.1056/NEJMoa1413462

Supplementary Appendix

Supplement to:

Inherited *DOCK2* Deficiency in Patients with Early-Onset Invasive Infections

Dobbs K, Domínguez Conde C, Zhang SY, Parolini S, Audry M, Chou J, Haapaniemi E, Keles S, Bilic I, Okada S, Massaad MJ, Rounioja S, Alwahadneh AM, Serwas NK, Capuder K, Çiftçi E, Felgentreff K, Ohsumi T, Pedergnana V, Boisson B, Haskoloğlu Ş, Ensari A, Schuster M, Moretta A, Itan Y, Patrizi O, Rozenberg F, Lebon P, Saarela J, Knip M, Petrovski S, Goldstein DB, Parrott RE, Savas B, Schambach A, Tabellini G, Bock C, Chatila T, Comeau AM, Geha RS, Abel L, Buckley RH, Íkincioğullari A, Al-Herz W, Helminen M, Doğu F, Casanova JL, Boztuğ K, Notarangelo LD.

Table of Contents

Supplementary Methods

Study subjects

The five index patients were from Lebanon (Patient 1), Finland (Patient 2), Turkey (Patient 3 and Patient 4) and Honduras/Nicaragua (Patient 5). They were included with informed written consent by the parents and approval from the Institutional Review Boards of Kuwait Ministry of Health, the INSERM Institute, the Rockefeller University, the Medical University of Vienna, Ankara University Medical School, Boston Children's Hospital, and the Duke University Medical School.

Genetic studies

The underlying genetic defects in the *DOCK2* gene were identified by whole exome sequencing (WES), with or without additional positional information generated by genome-wide linkage analysis (Patient 3) or homozygosity mapping (Patient 4). Genomic DNA was extracted from whole blood using the Gentra Puregene kit (Qiagen) for Patient 1 and Patient 5, the FlexiGene DNA kit (Qiagen) for Patient 2, the Qiamp midi DNA kit (Qiagen) for Patient 3, the Wizard Genomic DNA Purification kit (Promega) for Patient 4.

For Patient 3, four members of family 3 were genotyped with the Affymetrix genome-wide single nucleotide polymorphism (SNP) 6.0 array. Genotype calling was achieved with Affymetrix Power Tools (http://www.affymetrix.com/partners_programs/programs/developer/tools/powertools.affx) for the four family members. We discarded monomorphic SNPs, SNPs with a call rate lower than 100% and SNPs presenting more than one Mendelian inconsistency in the family. SNPs were further filtered with population-based filters. We then used about 111,600 high-quality SNP markers to carry out linkage analysis, assuming autosomal recessive inheritance with complete penetrance. Parametric multipoint linkage analysis was carried out with Merlin[1]. The Turkish family founders and HapMap CEU trios were used to estimate allele frequencies and to define linkage clusters, with an r^2 threshold of 0.4. For Patient 4, Affymetrix 6.0 SNP-based homozygosity mapping was performed to detect potential homozygous intervals. The protocol was carried out according to the Affymetrix® Genome-Wide Human SNP Nsp/Sty 6.0 protocol. Genotype calling was performed using the Affymetrix® Genotyping Console™ software. Detection and annotation of the

homozygous intervals was performed using HomozygosityMapper[2] and PLINK (http://pngu.mgh.harvard.edu/~purcell/plink/)[3].

For WES, Illumina paired-end libraries were created using the SureSelect Human All Exon V5 kit (Agilent), the Nextera exome enrichment kit (Illumina) and the Nimblegen SeqCap EZ V4.0.

For Patient 1 and Patient 2, libraries were sequenced using the Illumina HiSeq1500 sequencing platform with 101 bp read length. Average coverage of the exome for Patient 1 was 211x with 98% of the exome covered at a depth of ≥10x. The read mapping, variant calling and filtering steps for germ-line variants were performed as described previously[4].

For Patient 3, captured libraries were sequenced with the Illumina HiSeq2000 sequencing platform, and reads were mapped to the human reference genome assembly GRCh37 (UCSC hg19) using the Burrows-Wheeler Aligner (BWA)[5]. Variants were identified with the Genome Analysis Toolkit (GATK)[6], SAM tools[7] and Picard Tools (http://broadinstitute.github.io/picard/). Variant calls with a read coverage ≤2x and a Phred-scaled SNP quality ≤20 were eliminated.

For Patient 4, a multiplexed pool of twelve samples was sequenced on 4 lanes of the Illumina HiSeq2000 sequencing platform in 100 bp paired-end mode. Reads were aligned to GRCh37 using BWA, as indicated above. Duplicate reads were marked with Picard Tools (http://picard.sourceforge.net), while insertion/deletion realignment and base quality score recalibration was performed utilising the GATK. Variant calling was performed in the cohort of 12 samples using the GATK Unified Genotyper, before applying Variant Quality Score Recalibration (VQSR) (1000Genomes, HapMap, dbSNP131). All thresholds for GATK tools were based on the GATK Best Practice Variant Detection v3 recommendations[8].

For Patient 5, sequencing was completed on the Illumina HiSeq2500 sequencing platform in 125bp paired-end mode using KAPA Biosystem's library preparation kit followed by whole exome capture using Nimblegen SeqCap EZ V4.0. After processing the raw reads using a pipeline based on the GATK best practice protocol, the resulting alignments had ≥10-fold coverage in over 97.4% of the 33,266,994 bases of consensus coding sequence CCDS (release 14). The sequence data were analyzed using established protocols that identify qualifying variants forming genotypes not observed in a large control database of up to 61,486 samples provided by the Exome Aggregation Consortium (ExAC).

For all patients, candidate mutations were verified by capillary sequencing using BigDye chemistry (Life Technologies).

Sequence analysis

We used the SIFT[9], PolyPhen-2[10] and CADD[11] algorithms to assess the *in silico* predicted pathogenicity of the identified DOCK2 missense mutations.

T Cell Receptor Excision Circle (TREC) Assay

Dried blood spots collected at birth from Patient 2 and Patient 4 were retrieved upon informed consent. Real-time quantitative multiplex PCR was used to measure levels of TREC and RNaseP (as internal control) in template genomic DNA, as previously described[12].

Generation of T and NK cell lines

Peripheral blood mononuclear cells (PBMCs) were separated by Ficoll density gradient. For the generation of T cell lines, cells were activated and expanded *in vitro* using the human T cell activation/expansion kit according to manufacturer's instructions (Miltenyi). To obtain polyclonal NK cell lines, NK lymphocytes were isolated from PBMCs using negative selection (NK cell isolation Kit, Miltenyi), then cultured on irradiated feeder cells in the presence of 100 U/mL recombinant human IL-2 (Proleukin; Chiron) and 1.5 ng/mL phytohemagglutinin (GIBCO Ltd).

Western Blot

Whole cell lysates were prepared from 10^6 cells from control- and patient-derived T cell lines, loaded on 8-16% polyacrylamide TRIS-HEPES-SDS gel (Pierce Laboratories) and separated by SDS-PAGE. Proteins were transferred to polyvinylidene difluoride (PVDF) membrane using iBlot system (Invitrogen). Blots were probed overnight with 1:400 dilution of rabbit polyclonal anti-human DOCK2 (N-terminus) antiserum (AbCam), and 1:10,000 dilution of anti-β-Actin monoclonal antibody (Cell Signaling) as a loading control. Bands were revealed using SuperSignal West Femto kit (Fisher).

In a separate set of experiments, whole cell lysates were prepared from 10^6 cells from control- and patient-derived EBV-immortalized B cell lines, or SV40-immoralized

fibroblasts with or without stable expression of exogenous wild type DOCK2 expression through lentiviral transduction. Equal amounts of protein from each sample were separated by SDS-PAGE and blotted onto PVDF membrane (Bio-Rad, Hercules, CA), which was then probed with a goat anti-human DOCK2 antibody (R&D Systems, Minneapolis, MN), and with anti-GAPDH (Santa Cruz, California, CA) or anti-β-tubulin **(Sigma-Aldrich, St.Louis,** MO) antibodies as loading controls. Antibody binding was detected by enhanced chemiluminescence (ECL; Amersham-Pharmacia-Biotech).

In a separate set of experiments, whole cell lysates were prepared from HEK293T cells transiently transfected with either wild type DOCK2 or p.F744Cfs*27 mutant DOCK2 containing a Strep-HA tag at the N-terminus. Proteins were separated by SDS-PAGE and blotted onto PVDF membrane (Bio-Rad, Hercules, CA), which was probed with anti-HA-peroxidase conjugate antibody (Sigma Aldrich) and anti-GAPDH antibody (Santa Cruz Biotechnology). Antibody binding was detected by enhanced chemiluminescence (ECL; Amersham-Pharmacia-Biotech).

GTP-bound RAC1 pull-down assay

To evaluate TCR-induced RAC1 activation, 10^7 cells of patients and control-derived T cell lines were rested in culture medium overnight, then activated with or without 1 mg/ml anti-CD3 mAb (Miltenyi) for 30 min at 37°C. The cell lysates were then incubated with 20μg of Glutathione S transferase and GTPase binding domain of p21-activated kinase (GST-Pak1-PBD), immunoprecipitated with glutathione resin according to manufacturer's instructions (Pierce laboratories), and immunoblotted using anti-RAC1 monoclonal antibody (Pierce laboratories). Aliquots of the cell extracts were immunoblotted in parallel as loading controls.

Flow cytometry

For analysis of cell surface markers, $2x10^6$ PBMCs were used as starting material or 100 μl of whole blood in EDTA was lyzed using RBC Lysis Buffer (eBioscience). Cells were washed twice in FACS buffer (PBS with 2% FBS), and resuspended in 100 μl of FACS buffer with antibodies for 30 min on ice. Cells were washed twice in FACS buffer, resuspended in 300 μl of FACS buffer. The following monoclonal antibodies (mAbs) were used in various combinations for phenotypic analysis of T

and B lymphocytes: FITC-anti-CD3, PE-anti-CD4, PE-anti-CD16, APC-anti-CD8, APC-anti-CD56, APC-anti-CD31, APC-anti-CD24, PerCP Cy5.5-anti-CD19, PerCP Cy5.5-anti-CD3, PerCP Cy5.5-anti-CD45RA, PerCP Cy5.5-anti-CD45R0, PE Cy7-anti-CD3, Pacific Blue-anti-CCR7 (all from Biolegend), FITC-anti-CD45RA, FITC-anti-IgD, PE-anti-CD21, V450-CD8, V450-CD56, AF700-CD45RA, PE-Cy7-CD19 and APC-H7-CD3 (all from BD Biosciences), FITC-anti-CD57, FITC-anti-CD38, APC-anti-CD27, PerCP Cy5.5-anti-CD45, APC-anti-CD3, APC-anti-CD3 (all from eBioscience), PE-anti-IgM (from Southern Biotech), and PE-anti-CD4 and FITC-anti-CD16 (both from Beckman Coulter). Cells were analyzed on a LSR Fortessa (BD Biosciences). Data were analyzed with FlowJo software version 8.8.7 or version 10 (TreeStar).

For phenotypic analysis of NK lymphocytes, cells were first stained with appropriate primary mAbs, which included: anti-NKp46 (BAB281), anti-NKp30 (AZ20), anti-NKp44 (Z321 and AZ140), anti-NKG2D (ON72, BAT221, and ECM217), anti-CD16 (SUS142), anti-KIR2DL1/S1 (11PB6), anti-KIR2DL2/L3/S2 (GL183), anti-KIR3DL1/S1/L2 (AZ158), anti-NKG2A (Z199), anti-CD57 (XA147). Cells were then stained with PE-conjugated isotype-specific goat-anti-mouse antiserum (Southern Biotechnology, Birmingham, AL), followed by staining with a mixture of FITC-labeled anti-CD3, FITC-anti-CD14, FITC-anti-CD20 and PC5-anti-CD56. Analysis of NK cell markers was performed by gating on $CD56^{+}CD3^{-}CD14^{-}CD20^{-}$ cells. Cells were analyzed on a FACSCanto (BD Biosciences). Data were analyzed with Diva v6.1.3 software (BD Biosciences, Mountain View, CA). All primary mAbs used for NK cell phenotyping were generated at the Department of Molecular and Translational Medicine, University of Brescia, Italy and in the Laboratory of Molecular Immunology, DIMES, University of Genoa, Italy, and have been previously described[13].

For the analysis of NKT lymphocytes, PBMCs were stained with PE-Texas red or FITC- conjugated CD45, APC/Cy7 or PerCP5.5-conjugated CD3, FITC or PECy7-conjugated CD4, APC or APC/Cy7-conjugated CD8, and PE or APC-conjugated, PBS57-loaded, CD1d-tetramers (with unloaded CD1d tetramers used as control). Upon gating on $CD45^{+}$ cells, NKT cells were identified as $tetramer^{+}$ $CD3^{+}$. Events were collected on a BD Canto flow cytometer (BD Biosciences) and analyzed with FlowJo software, version 8.8.7. CD1d-tetramers were obtained from National Institute

of Allergy and Infectious Disease Major Histocompatibility Complex Tetramer Core Facility, Atlanta, GA.

Analysis of NK cell degranulation and IFN-γ production.

For degranulation assay against erythroleukemia human cell line K562 and mastocytoma murine cell line P815, PBMCs derived from Patient 1 and Patient 2 and from healthy controls were incubated with or without 100 U/mL recombinant human IL-2 (Proleukin; Chiron) at 37°C overnight (in the case of K562 target cell assay) or for three days (for P815 target cell assay). Cells were then incubated with target cells at an effector:target ratio of 1:2 (for K562 cells) and 1:7 (for P815 cells), in a final volume of 200 μl in round-bottomed 96-well plates at 37°C and 5% CO2 for 4 hours in culture medium supplemented with anti-CD107a-PE monoclonal antibody. Degranulation assay was performed in the absence or presence of various mAbs including anti-NKp30, anti-NKp46, anti-Nkp44, anti-CD16, anti-NKG2C and anti-NKG2D, respectively. After 1 h of co-incubation, GolgiStop (BD Biosciences Pharmingen, San Diego, CA, USA) was added at a 1:100 dilution. Surface staining was done by incubating the cells with anti-CD3, anti-CD14, anti-CD20 and anti-CD56 mAbs for 30 min at 4°C. The cells were washed and analyzed by flow cytometry (FACSCanto, BD Biosciences). Analysis of NK cell degranulation was performed by gating on $CD56^{+}CD3^{-}CD14^{-}CD20^{-}$ cells and analyzing the proportion of cells expressing CD107a on the cell surface. The re-directed killing assay against P815 target cells was also performed using polyclonal NK cells that had been grown *in vitro* as described above.

To detect intracellular production of IFN-γ, PBMCs derived from Patient 2 and from healthy controls were incubated overnight at 37°C with IL-12 (0.5 ng/ml), or IL-12 (0.5 ng/ml) and IL-18 (0.1 ng/ml) combined. Cells were then washed, fixed and permeabilized with BD Cytofix/Cytoperm kit (BD Biosciences Pharmingen). IFN-γ production was detected by subsequent intracellular staining with anti-IFN-γ-PE (BD Biosciences Pharmingen) upon gating on $CD56^{+}CD3^{-}CD14^{-}CD20^{-}$ cells.

For both degranulation and IFN-γ expression experiments, the percentage of positive cells was calculated subtracting the baseline CD107a or IFN-γ expression in control cultures in the absence of stimuli (target cells or cytokines).

Chemotaxis assay

$5x10^5$ PBMCs from patients and healthy controls were suspended in 100 µL RPMI media with 10% FBS. The cells were loaded into 5.0 µm Transwell inserts (Corning) which were placed onto 24-well plates containing 450 mL of RPMI medium alone or supplemented with 1.5µg/mL CCL21 or with 800ng/mL CXCL12 (Peprotech). After 3 hours of incubation at 37°C, cells that had migrated to the lower chamber were collected, stained with PerCP-Cy5.5 labeled anti-CD19 and with APC-conjugated anti-CD3 (both from Biolegend) and counted by flow cytometry (BD Fortessa). Results were calculated as percentage of cells that had migrated out of total input cells.

F-Actin Polymerization

For analysis of chemokine-induced actin polymerization in T and B lymphocytes, PBMCs ($2.5x10^6$ cells/mL in RPMI, 1% FCS) were allowed to rest at least 3 hours on ice, then stimulated with 800 ng/ml CXCL12. Aliquots were taken at the indicated time points (between 0 and 60 seconds), and immediately fixed in 4% paraformaldehyde for 10 min. After washing with PBS and FcgR blocking with human serum (1:10 dilution in PBS), cells stained with FITC-conjugated anti-CD3 and PerCP-Cy5.5 labeled anti-CD19 mAb (BioLegend), permeabilized using BD Cytofix/Cytoperm Kit, stained with AlexaFluor 647-conjugated phalloidin (Molecular Probes), and analyzed by flow cytometry (BD Fortessa) using FlowJo software version 8.8.7 (TreeStar).

For analysis of actin polymerization in NK lymphocytes, 10^5 polyclonal IL2-activated NK cells/tube were re-suspended in 100 µl RPMI media and rested overnight in RPMI without IL-2. After 30 min incubation on ice, cells were incubated with CD16- and NKp46-specific primary antibodies on ice for one hour, then warmed at 37°C for 2 min, incubated and cross-linked with isotype-specific secondary antibodies for 30s and fixed with 4% paraformaldehyde for 10 min. After washing with PBS, cells were re-suspended in 200 µl of Fix/Perm solution (BD Biosciences) at 4°C for 20 min, washed twice with 0.1% saponin solution, stained with CF^{TM}633 Dye-conjugated phalloidin (Biotium) (1:400 dilution in saponin) at 4°C for 30 minutes and then re-suspended in 500 µl of PBS solution for flow cytometry analysis. Events were acquired on BD Fortessa, and analyzed with FlowJo software version 8.8.7 (TreeStar). Results were expressed as phalloidin mean fluorescence intensity (MFI) at

each time point.

Flow cytometry analysis of ERK1/2 and MEK1 phosphorylation

10^5 polyclonal IL2-activated NK cells/tube were re-suspended in 100 µl RPMI media, rested for 48 hours in RPMI without IL-2, and incubated at 4°C for 15 min. Cells were then incubated for 1 hour at 4°C with various primary antibodies specific for CD16, NKp30 and NKp46. After cross-linking stimulation with isotypic specific secondary antibodies for 3-5 min, the cells were incubated with 200 µl of Fix/Perm solution (BD Biosciences) at 4°C for 20 min, washed twice with 0.1% saponin solution, then stained for 30 minutes at 4°C with Alexa Fluor 488 Mouse Anti-ERK 1/2 – pT202/pY204 or with Alexa Fluor 488 Mouse Anti-MEK 1 – pS298 (both from BD Biosciences), and re-suspended in 500 µl of PBS. Events were acquired on BD Fortessa, and analyzed with FlowJo software version 8.8.7 (TreeStar).

Cytokine production

To measure cytokine production, PBMCs isolated by Ficoll-Paque density gradient centrifugation were stimulated with intact viruses for 24 hours, at a concentration of 2×10^6 cells/ml in RPMI 1640 supplemented with 10% FCS. We used herpes simplex virus-1 (HSV-1, strain KOS-1, multiplicity of infection (MOI)=1), and vesicular stomatitis virus (VSV, strain Indiana, MOI=1). The production of IFN-α, -β, -λ and IL-6 was assessed by ELISA. ELISA for IFN-α (AbCys SA, Paris, France), IFN-β (TFB, Fujirebio, Inc., Tokyo, Japan), and IL-6 (Sanquin, Amsterdam), respectively, was carried out according to the kit manufacturer's instructions. The IFN-λ ELISA was developed in the laboratory. Briefly, plates were coated by incubation overnight at 4°C with 1 µg/ml of anti-human IFN-λ1 monoclonal antibody (R&D Systems, Minneapolis, MN), and the IFN-λ1 concentration in the supernatant was measured using a secondary biotinylated anti-human IFN-λ1 monoclonal antibody (R&D Systems, Minneapolis, MN) at a concentration of 400 µg/ml.

Determination of mRNA levels by RT-qPCR

Total RNA was extracted from PBMCs. RNA was reverse-transcribed directly, with random hexamers, to determine mRNA levels for different subtypes of IFNA, IFNB, IFNL1, IFIT1, MX1 and IL6. Reverse transcription-quantitative PCR (RT-qPCR) was

performed with Applied Biosystems Assays-on-Demand™ probe/primer combinations and 2 x universal reaction mixture, in an ABI PRISM® 7700 Sequence Detection System. We used β-glucuronidase (GUS) for normalization. Results are expressed according to the ΔΔCt method, as described by the manufacturer.

Viral replication in fibroblasts and effects on cell viability

10^5 SV40-fibroblasts were plated in individual wells of 24-well plates and infected with vesicular stomatitis virus (VSV), at a MOI of 0.1, in DMEM medium supplemented with 2% FCS. After 30 minutes, cells were washed and incubated in 500 µl of medium. Supernatants were obtained at the 2h, 8 h, 16h, 24h and 48 h time points and frozen. VSV titers were determined by calculating the 50% end point ($TCID_{50}$) after the inoculation of Vero cell cultures in 96-well plates.

The viability of SV40-fibroblasts upon VSV or EMCV infection was assessed by resazurin oxidoreduction (TOX-8) (Sigma-Aldrich, St. Louis, Missouri). Cells were plated in triplicates in 96-well flat-bottomed plates (2 x 10^4 cells/well) in DMEM supplemented with 10% FCS; 18 hours later, cells were infected by incubation for 24 hours with VSV at the indicated MOI. Resazurin dye solution was then added, at a volume one tenth that of the culture medium, and the samples were incubated for an additional two hours at 37°C. Fluorescence was then measured at a wavelength of 590 nm, using an excitation wavelength of 560 nm. Background fluorescence, calculated for dye and complete medium alone (in the absence of cells) was then subtracted from the values for all the other samples; 100% viability corresponds to the fluorescence of uninfected cells. For assays of cell protection upon viral stimulation, cells were treated with IFN-α2b (Schering-Plough, Brussels, Belgium, 1 x 10^3 IU/ml), starting the same time as infection

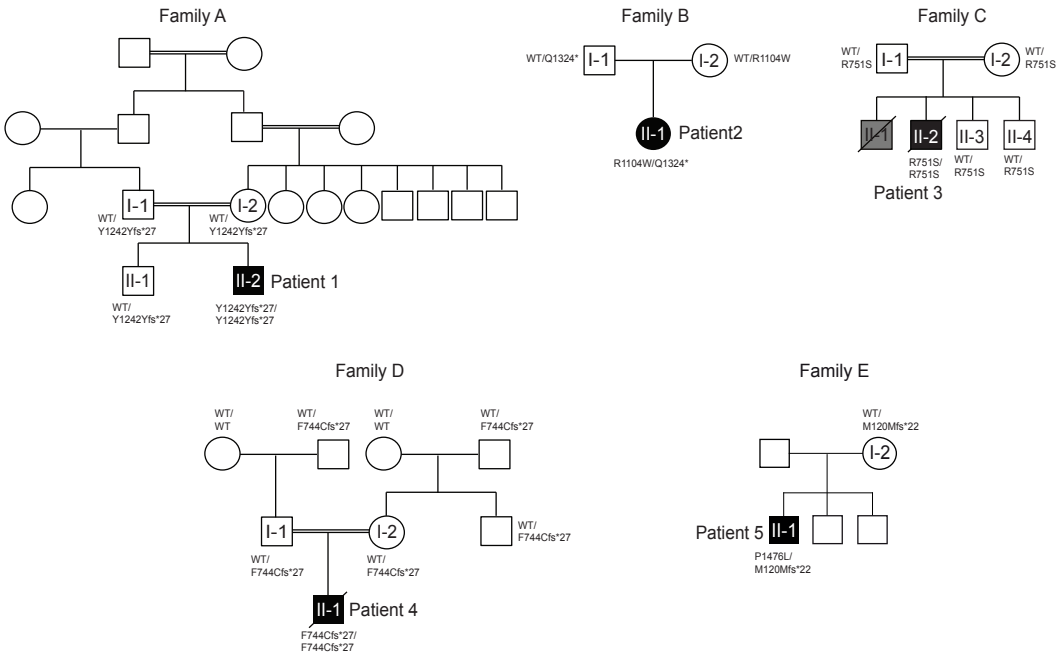

Figure S1. Segregation of *DOCK2* mutations. Extended patient pedigrees showing the segregation of the identified *DOCK2* mutations. In all pedigrees, the identified *DOCK2* mutations fully segregate with the disease phenotype under the assumption of autosomal recessive inheritance with full penetrance. Since no DNA was available from Patient 5's father, the possibility of the *DOCK2* p.P1476L mutation being a *de novo* mutation cannot be ruled out.

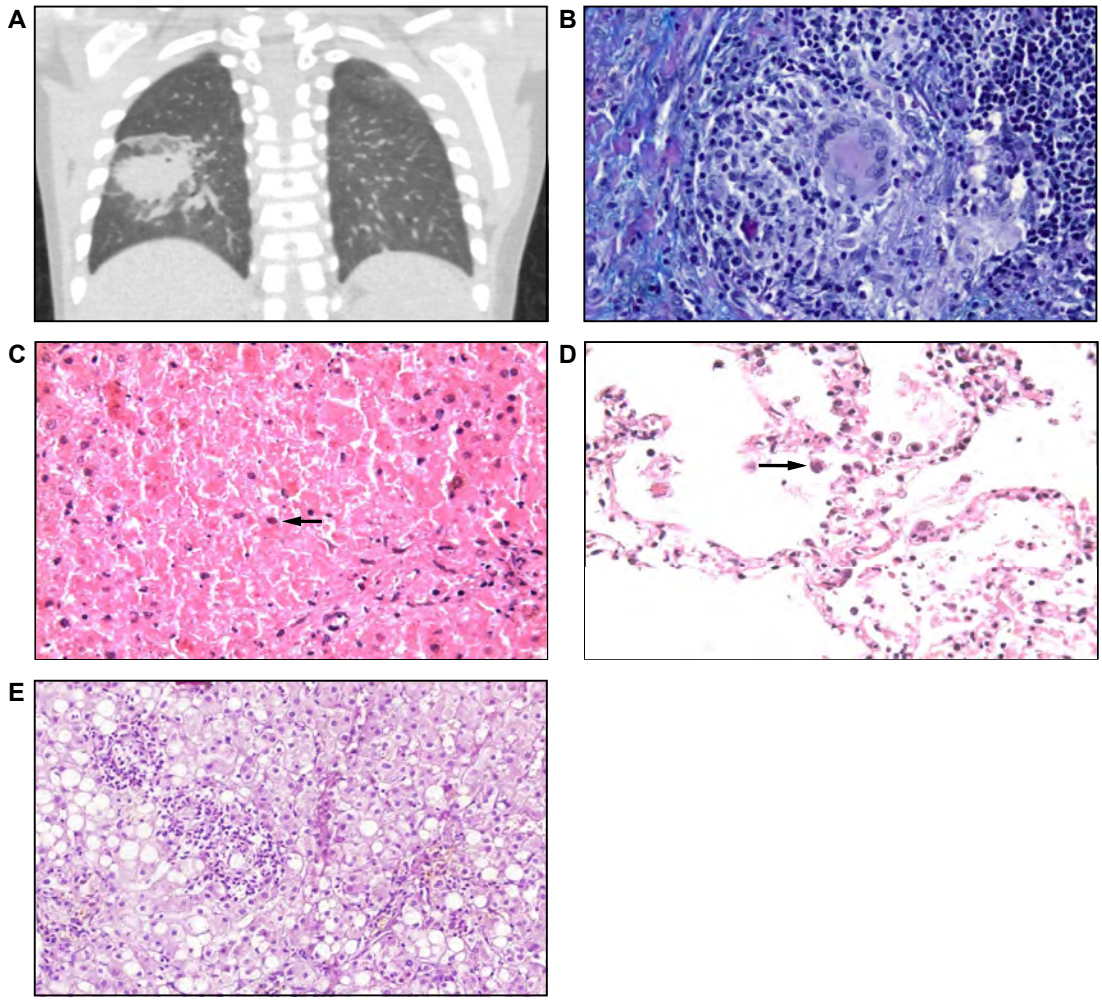

Figure S2. Clinical features identified in DOCK2-deficient patients. (A) CT scan of the lung showing granuloma in Patient 2. (B) Lung immunopathology showing granuloma in Patient 2. (C) Postmortem histology of a liver specimen from Patient 3 showing a degraded hepatocyte with a nuclear inclusion (black arrow). The background liver parenchyma is necrotic. (D) Postmortem histology of lung specimen from Patient 3 showing polymorphonuclear leukocytes and necrotic fragments in the alveolar spaces. A cell with a nuclear inclusion (black arrow) is indicated. Both C and D: hematoxylin/eosin staining, magnification 400x. (E) Liver biopsy showing significant hepatocyte macroversicular fatty change, lobular and portal inflammation with eosinophils, yellow-brown pigment accumulation in Patient 4 (hematoxylin/eosin staining, magnification 200x).

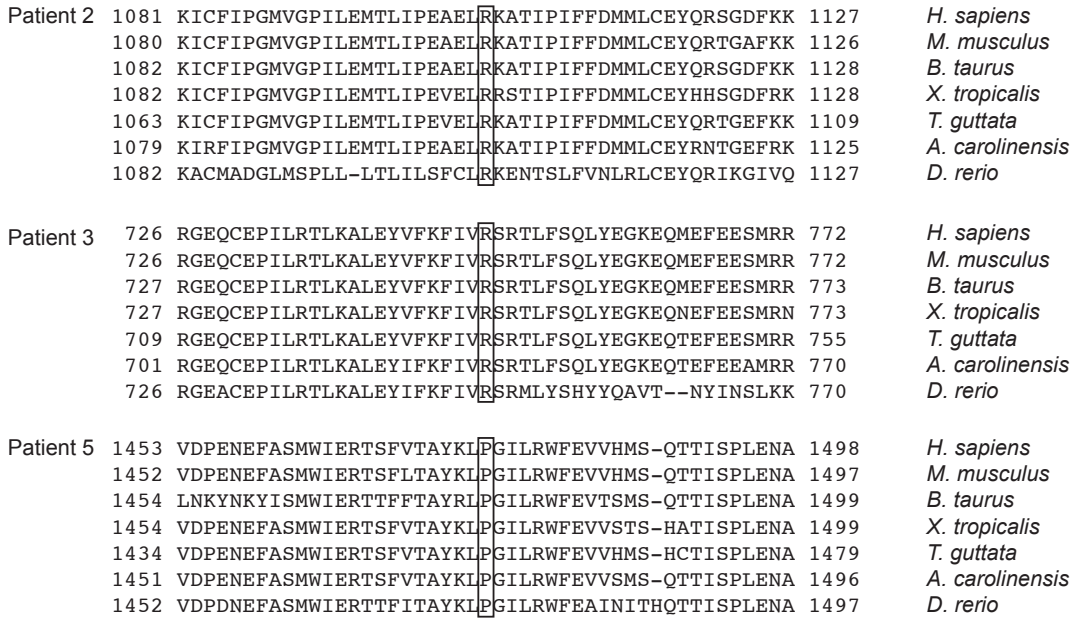

Figure S3. Evolutionary conservation of the amino acids affected by the identified *DOCK2* missense mutations. Amino-acid sequence of the region containing residues R751, R1104 and P1476 (all three indicated by a black frame) mutated in Patient 3, Patient 2, and Patient 5 respectively, illustrating that the positions affected by the mutations have been conserved throughout evolution.

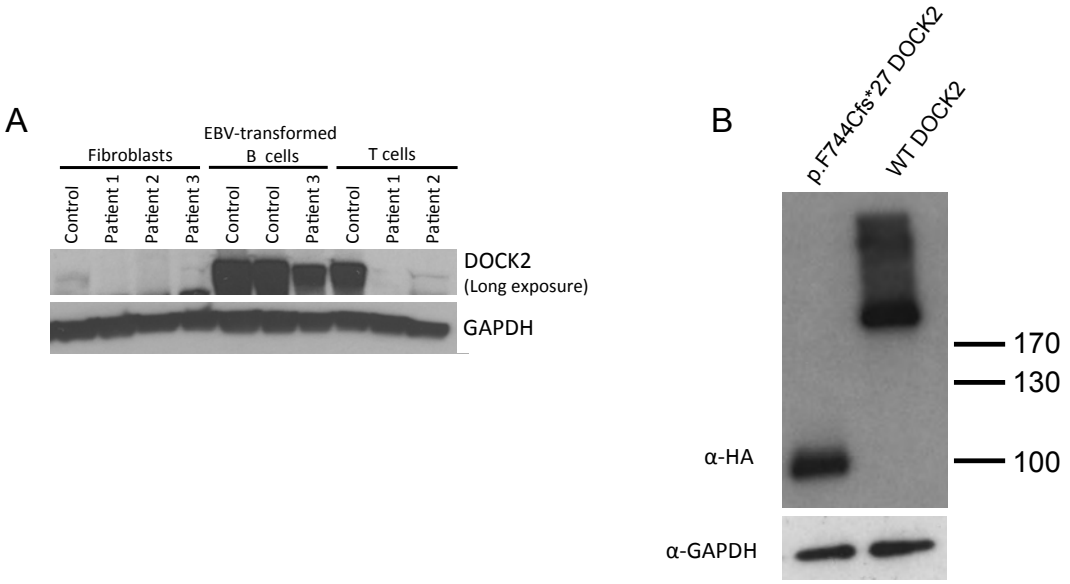

Figure S4. Western blot analysis of DOCK2 expression. Panel A shows Western blot analysis of SV-40-immortalized primary fibroblasts derived from Patient 1, Patient 2 and Patient 3, EBV-immortalized B-cell lines derived from Patient 3 and T cells derived from Patient 1 and Patient 2 showing absence or severely reduced expression of DOCK2 protein, in comparison with those from two healthy controls. GAPDH was used as a loading control. Panel B shows Western blot analysis of HEK293T cells transiently transfected with a vector containing Strep-HA tagged wild-type DOCK2 or p.F744Cfs*27 mutant DOCK2. GAPDH was used as a loading control.

Figure S5

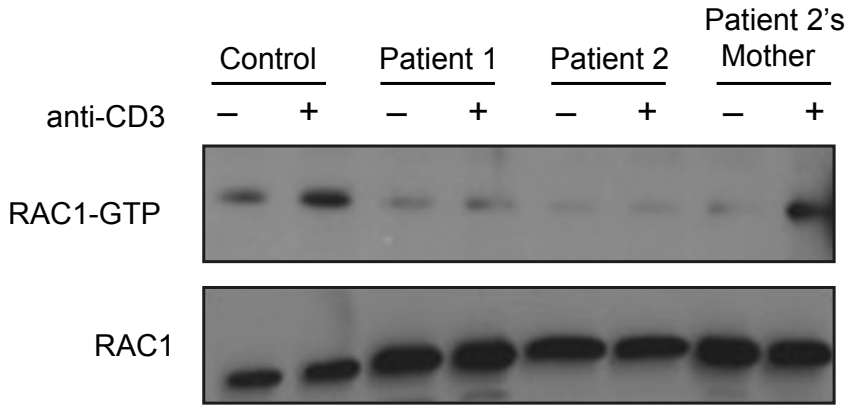

Figure S5. RAC1 activation pull-down. Defective RAC1 activation in T-cell lines derived from Patient 1 and Patient 2 upon stimulation of the T-cell receptor with anti-CD3 monoclonal antibodies. The figure displays the raw data used to generate the bar graph shown in Figure 2A.

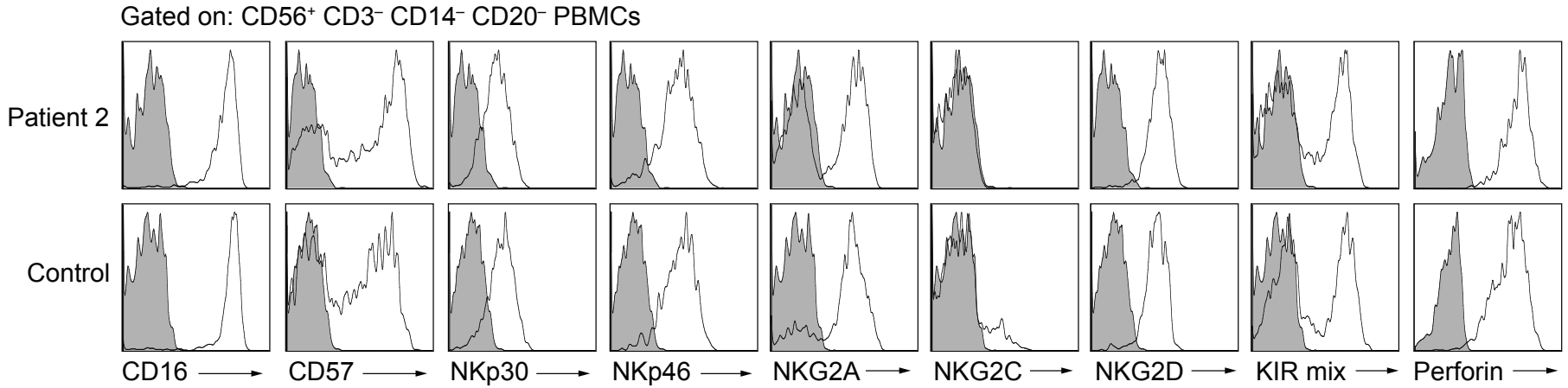

Figure S6. Phenotypic analysis of circulating NK cells. Expression of cell surface molecules and intracellular perforin on $CD3^-$ $CD56^+$ NK cells analyzed by flow cytometry. KIR mix – a cocktail of monoclonal antibodies recognizing KIR2DL1, KIR2DL3 and KIR3DL2.

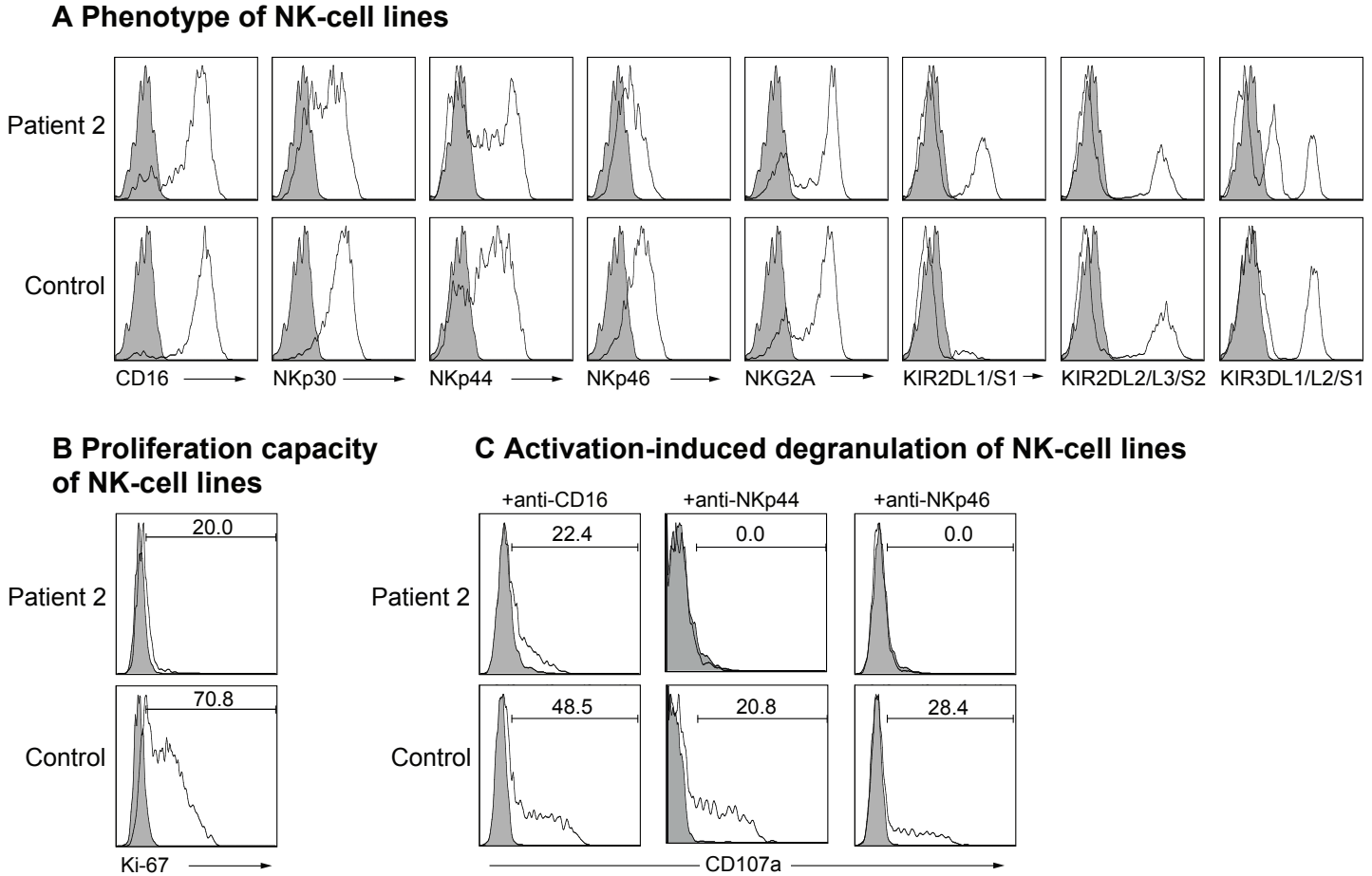

Figure S7. Phenotype, proliferation capacity and activation-induced degranulation of patient-derived IL-2-activated (100U/ml) polyclonal NK-cell lines. (A) Cell surface expression of NK-cell surface markers. (B) Representative flow cytometry histograms showing proliferation capacity of Patient 2-derived NK-cell line cultured in the presence of IL-2. (C) Impaired CD107a expression on cell surface of Patient 2-derived, IL-2-activated polyclonal NK-cell line upon engagement of CD16, NKp44 and NKp46, respectively. The numbers in the gates denote the increase in the percentage of $CD107a^{+}$ cells upon stimulation (solid line histograms) compared to unstimulated controls (grey histograms).

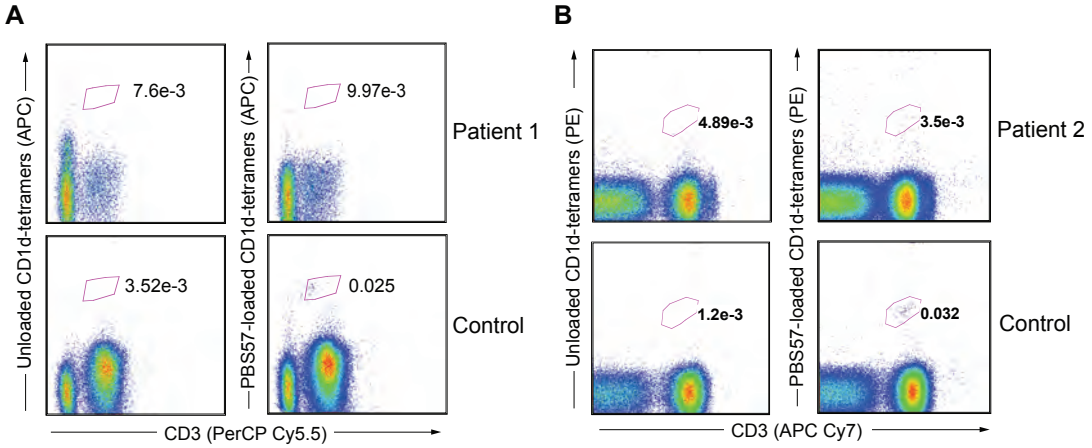

Figure S8. Identification of NKT cells in DOCK2-deficient patients. Flow cytometry analysis of CD1d-tetramer staining of $CD3^+$ PBMCs from Patient 1 and Patient 2, illustrating absence of NKT cells in the DOCK2-deficient patients.

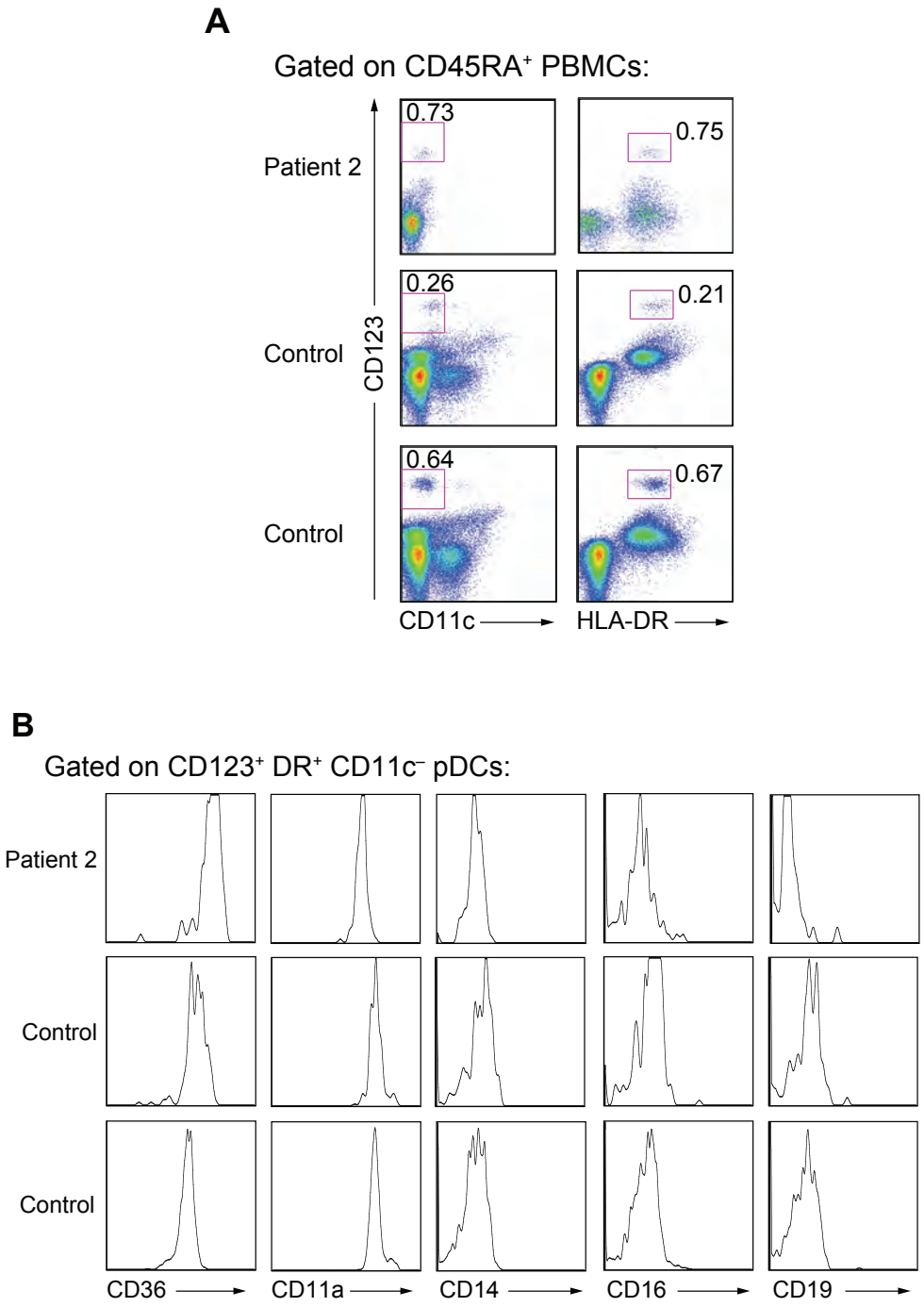

Figure S9. Identification and phenotypic characterization of plasmacytoid DCs (pDCs) in Patient 2. (A) Flow cytometry dot-plots showing comparable relative numbers of $CD123^+$ $HLA\text{-}DR^+$ $CD11c^-$ pDCs (within the normal range) in PBMCs from Patient 2 and two healthy controls. (B) Unaltered cell-surface marker expression on pDCs from Patient 2 and two healthy controls, shown by the representative flow cytometry histograms.

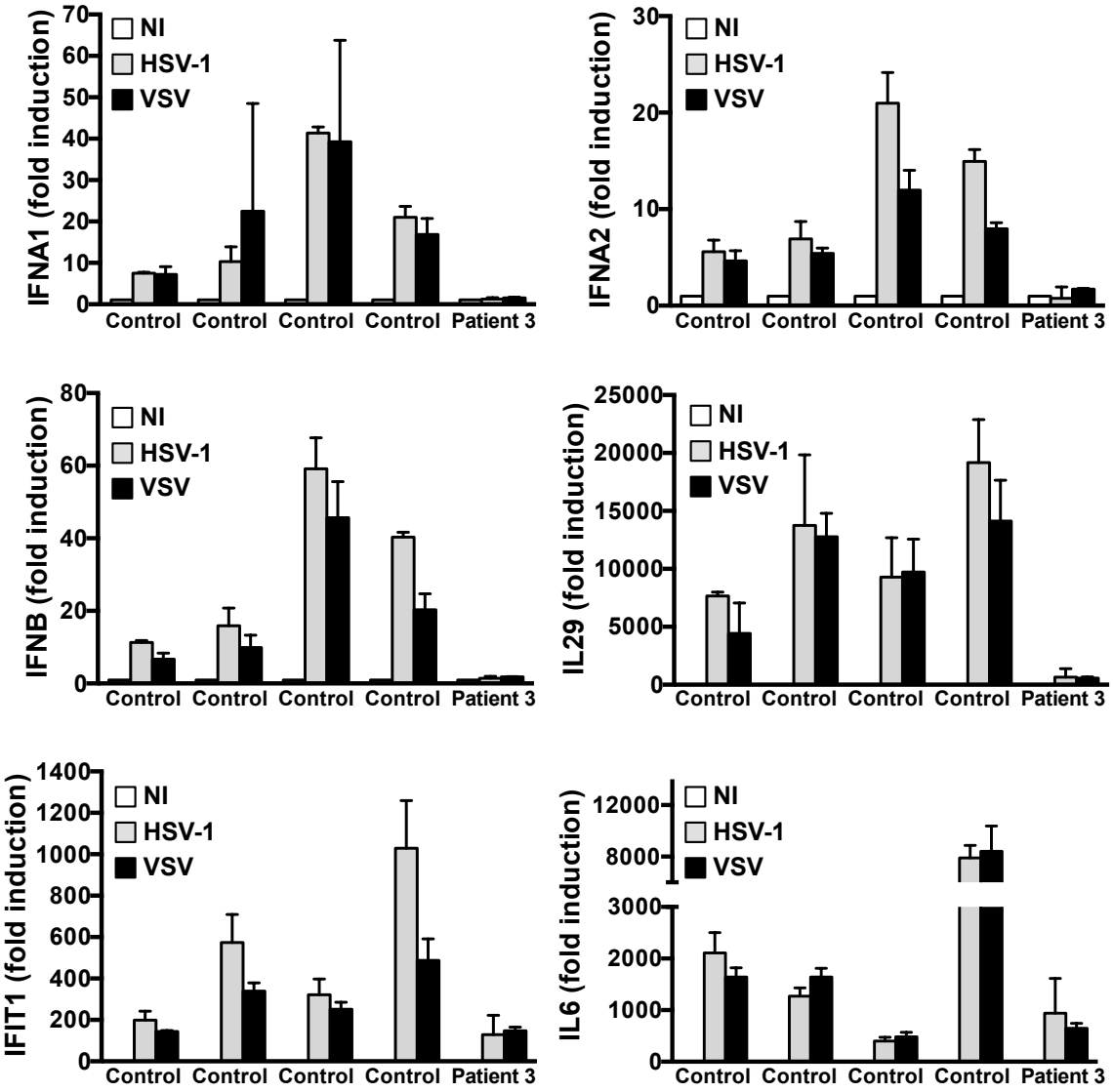

Figure S10. Induction of indicated gene transcription levels upon viral infection *in vitro*. NI, not infected. The induction of *IFNA1, IFNA2, IFNB, IL29, IFIT1* and *IL6* was measured by RT-qPCR, in PBMCs from Patient 3 and four healthy controls, with and without infection with HSV-1 or VSV.

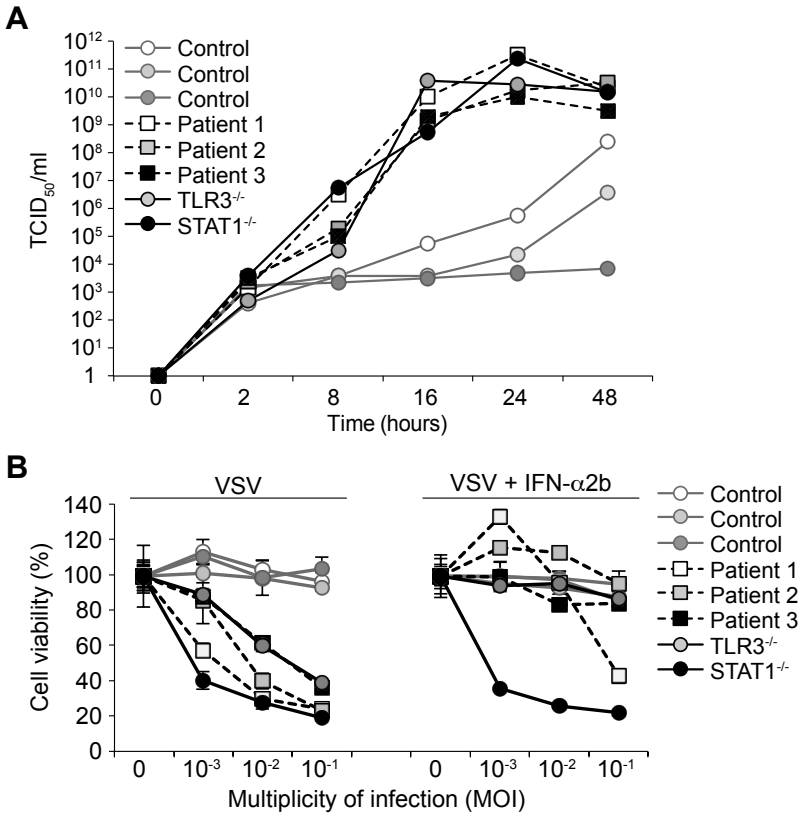

Figure S11. Impaired antiviral interferon responses in patient-derived DOCK2-deficient fibroblasts. (A) High levels of VSV (vesicular stomatitis virus) replication in DOCK2-deficient SV40 fibroblasts from Patient 1, Patient 2 and Patient 3, and in SV40 fibroblasts from healthy controls. $TCID_{50}$ – median tissue culture infective dose. (B) VSV-induced cell death of DOCK2-deficient SV40 fibroblasts (left panel) and the rescue of the VSV-induced cell death by addition of IFN-α2b (right panel).

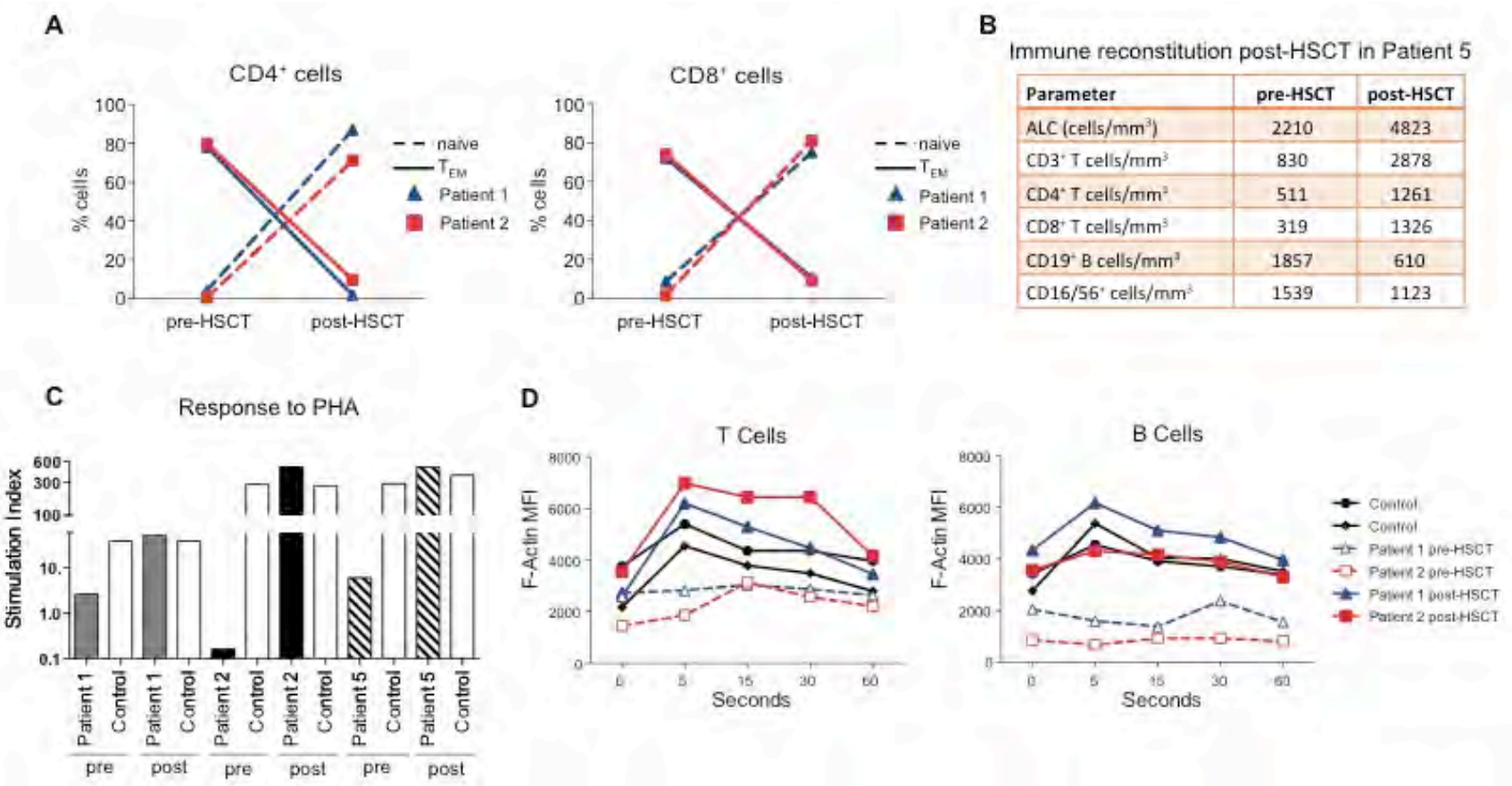

Parameter	pre-HSCT	post-HSCT
ALC (cells/mm³)	2210	4823
CD3⁺ T cells/mm³	830	2878
CD4⁺ T cells/mm³	511	1261
CD8⁺ T cells/mm³	319	1326
CD19⁺ B cells/mm³	1857	610
CD16/56⁺ cells/mm³	1539	1123

Figure S12. Normalization of T-cell subset distribution, PHA response and actin polymerization after HSCT. (A) Relative numbers of naïve (dashed line) and effector memory (solid line) $CD4^+$ and $CD8^+$ T cells after allogeneic hematopoietic stem cell transplantation (HSCT)in Patient 1 (blue triangles) and Patient 2 (red squares). (B) Absolute cell counts before and HSCT in Patient 5. (C) Response of Patient 1 (grey bars), Patient 2 (filled bars) and Patient 5 (dashed bars) peripheral blood mononuclear cells to stimulation with phytohemagglutinin pre- and post-HSCT. (D) Normalization of CXCL12-induced actin polymerization after HSCT in T cells (left) and B cells (right).

Table S1. Variants identified by exome sequencing in patients Patients 1-5. Homozygous variants identified in patients Patient 1, Patient 3, and Patient 4 and not found in public (dbSNP, 1000 genomes) or in-house databases are shown in the upper table. Homozygous variants and heterozygous variants identified in the same gene identified in Patient 2 and not found in public (dbSNP, 1000 genomes) or in-house databases are shown in the lower table. Non-synonymous homozygous variants and heterozygous variants in the same gene identified in Patient 5 and not reported in homozygous form, or present at an allelic frequency greater than 1% among public (ExAC consortium) or in-house databases are displayed in the lower table.

Patient	Chr.	Start	Reference	Genomic variant in patient	Gene
Patient 1					
	1	38077349	-	A	*RSPO1*
	1	38077420	-	CC	*RSPO1*
	1	54605319	-	C	*CDCP2*
	1	154530774	C	A	*UBE2Q1*
	1	156035733	G	C	*RAB25*
	1	156571221	C	G	*GPATCH4*
	1	160062156	C	T	*IGSF8*
	1	160062977	G	A	*IGSF8*
	1	240255583	CGG	-	*FMN2*
	2	23926150	G	A	*KLHL29*
	2	27278084	A	G	*AGBL5*
	2	29274911	-	AGAGGGGTGGCC	*FAM179A*
	2	29293863	GGG	-	*C2orf71*
	2	42990200	G	A	*OXER1*
	2	88751752	-	G	*FOXI3*
	2	175292599	TTTATCAGTCAAA	-	*SCRN3*
	2	231033633	ATTTTTTTTTTTTTT	ATTAATTTTTTTTTTTTTTT	*SP110*
	2	233351330	C	T	*ECEL1*
	3	16926567	T	C	*PLCL2*
	3	50306757	-	C	*SEMA3B*
	3	53324829	CACTGG	-	*DCP1A*
	3	63898392	-	AGCAGC	*ATXN7*
	3	133969438	-	G	*RYK*
	3	133969490	-	C	*RYK*
	3	141162449	C	T	*ZBTB38*
	4	3076657	GCAGCA	-	*HTT*
	4	155244425	GTTT	-	*DCHS2*
	5	72743299	-	GC	*FOXD1*
	5	167881041	AGG	-	*WWC1*

5	169122829	A	G	*DOCK2*
5	169468118	-	TA	*DOCK2*
5	176930176	AGG	-	*DOK3*
6	27223069	AGAGCCAGATTAAGG	-	*PRSS16*
6	161519381	CTG	-	*MAP3K4*
7	128587374	GGCCGCCTACTCTGCAGCCGCCCACTCTGC	-	*IRF5*
7	150783917	T	G	*AGAP3*
8	33354255	-	TGA	*MAK16*
8	65494050	-	GCA	*BHLHE22*
8	144511981	TGG	-	*MAFA*
9	79318378	GACAGCCTGCAACGT	-	*PRUNE2*
9	95237066	ATC	-	*ASPN*
9	96439006	-	TGCCTCCACCACACC	*PHF2*
9	123476563	GCGGCG	-	*MEGF9*
10	11374612	CCAGTCTTCCTCTTCGGCATGCCCTGGAAGCTTCTT	-	*CELF2*
10	73499446	A	G	*CDH23*
10	74673110	A	G	*OIT3*
10	74953294	C	G	*FAM149B1*
11	65636053	T	C	*EFEMP2*
12	6777111	CTG	-	*ZNF384*
12	53184620	-	A	*KRT3*
13	72440684	CCGCCG	-	*DACH1*
14	77493761	TTGCTGCTGCTGCTGCTGCTGCTGCTGCTGTTGCTGCTGCTGCTGCTG	TTGCTGCTGCTGCTGCTGCTGCTGTTGCTGCTGCTGCTGCTG	*IRF2BPL*
15	31776229	GGC	-	*OTUD7A*
15	102029688	-	CG	*PCSK6*
16	31099000	C	T	*PRSS53*
16	31508241	G	A	*C16orf58*
16	48120692	A	G	*ABCC12*
16	67241587	C	T	*LRRC29*
17	8384692	C	T	*MYH10*
17	21156532	-	C	*C17orf103*
17	46115074	-	G	*COPZ2*
17	46115123	-	G	*COPZ2*
17	48227384	GC	GGCC	*PPP1R9B*
19	4511548	A	T	*PLIN4*
19	4817312	-	AGG	*TICAM1*
19	8389898	CTC	-	*KANK3*
19	9073059	G	C	*MUC16*
19	14200896	-	G	*SAMD1*
19	18717401	CAG	-	*CRLF1*
19	37879852	CCA	CTGTGCA	*ZNF527*
19	49956468	ACCCCATTCCCATTAGCCCC	-	*ALDH16A1*

	19	50832152	T	C	*KCNC3*
	19	52400146	C	T	*ZNF649*
	19	55944675	C	T	*SHISA7*
	20	32664865	-	AGC	*RALY*
	20	35807793	-	ATAGACAGGGCCCCGC GGCCGGCACTCTT	*C20orf132*
	22	20780030	-	C	*SCARF2*
	22	50655681	G	A	*SELO*
Patient 3					
	3	108269959	A	G	*KIAA1524*
	5	112312899	G	C	*DCP2*
	5	140433373	G	A	*PCDHB1*
	5	149215910	A	T	*PPARGC1B*
	5	149772948	G	A	*TCOF1*
	5	150029416	G	A	*SYNPO*
	5	156635924	A	G	*ITK*
	5	169145781	G	T	*DOCK2*
	5	170640698	T	G	*RANBP17*
	9	130635140	C	T	*AK1*
	17	7756658	G	A	*KDM6B*
Patient 4					
	1	248790341	G	A	*OR2T11*
	5	169145753	A	ATG	*DOCK2*
	5	169291354	TCTG	T	*FAM196B*
	9	130117713	CCT	C	*GARNL3*
	9	130164952	C	T	*SLC2A8*
	9	136208374	C	T	*MED22*
	9	139934469	TCC	T	*NPDC1*

Patient	Chr.	Start	Reference	Zygosity	Genomic variant in patient	Gene
Patient 2						
	1	152195728	T	homo	TT	*HRNR*
	2	95847040	-	homo	GCG	*ZNF2*
	2	187559029	-	homo	GCAGCA	*FAM171B*
	3	195452870	G	het	A	*MUC20*
	3	195452872	AG	het	CA	*MUC20*
	4	3076603	-	homo	GCA	*HTT*
	4	147560450	-	homo	TGG	*POU4F2*
	5	169446041	C	het	T	*DOCK2*
	5	169474517	C	het	T	*DOCK2*
	5	171201610	A	het	C	*CTB-78H18.1*
	5	171201615	A	het	C	*CTB-78H18.1*
	9	132630664	GAC	homo	-	*USP20*
	10	50534969	-	homo	ACACACAC	*C10ORF71*
	12	21791410	A	homo	-	*LDHB*
	16	1823389	G	homo	-	*EME2*
Patient 5						
	5	169101338	-	het	GATGTAC	*DOCK2*
	5	169484630	C	het	T	*DOCK2*
	11	74203186	G	homo	A	*LIPT2*
	11	125887165	G	het	A	*CDON*
	11	125891299	C	het	T	*CDON*
	18	29027853	T	het	C	*DSG3*
	18	29054099	C	het	T	*DSG3*

Note that for Patient 5 we have listed all putative compound heterozygous variants, however, it is likely that both identified heterozygous variants in *CDON* and *DSG3* are paternal alleles since exome sequencing data for the mother of Patient 5 showed none of the two reported variants in each of these genes.

Table S2. Predicted impact of the identified *DOCK2* missense mutations. The mutations were scored using the SIFT, PolyPhen-2 and CADD algorithms. None of the *DOCK2* mutations identified in the affected patients were found in public (dbSNP, 1000 genomes, NHLBI exomes) or our private databases comprising over 2,000 exomes; however, the p.Q1324* allele was present in a large dataset containing >3,500 Finnish exomes at minor allele frequency (MAF) of 0.0002[14] and as heterozygous variant in the ExAC database with a MAF of 0.0001512, the p.R1104W was present as heterozygous variant in the ExAC database with a MAF of 0.00001499 and the p.P1476L was present as heterozygous variant in the ExAC database with a MAF of 0.00009615.

***DOCK2* mutation**	**SIFT score**	**PolyPhen-2 score**	**CADD score**
p.R1104W	0.000	0.983	19.29
p.R751S	0.03	0.991	17.76
p.P1476L	0.000	1.000	32

Supplementary References

1. Abecasis GR, Cherny SS, Cookson WO, Cardon LR. Merlin--rapid analysis of dense genetic maps using sparse gene flow trees. Nat Genet 2002;30:97-101.
2. Seelow D, Schuelke M, Hildebrandt F, Nurnberg P. HomozygosityMapper--an interactive approach to homozygosity mapping. Nucleic Acids Res 2009;37:W593-9.
3. Purcell S, Neale B, Todd-Brown K, et al. PLINK: a tool set for whole-genome association and population-based linkage analyses. Am J Hum Genet 2007;81:559-75.
4. Sulonen AM, Ellonen P, Almusa H, et al. Comparison of solution-based exome capture methods for next generation sequencing. Genome biology 2011;12:R94.
5. Li H, Durbin R. Fast and accurate short read alignment with Burrows-Wheeler transform. Bioinformatics 2009;25:1754-60.
6. McKenna A, Hanna M, Banks E, et al. The Genome Analysis Toolkit: a MapReduce framework for analyzing next-generation DNA sequencing data. Genome Res 2010;20:1297-303.
7. Li H, Handsaker B, Wysoker A, et al. The Sequence Alignment/Map format and SAMtools. Bioinformatics 2009;25:2078-9.
8. Van der Auwera GA, Carneiro, M.O., Hartl, C., Poplin, R., del Angel, G., Levy-Moonshine, A., Jordan, T., Shakir, K., Roazen, D., Thibault, J., Banks, E., Garimella, K.V., Altshuler, D., Gabriel, S., DePristo, M.A. . From FastQ Data to High-Confidence Variant Calls: The Genome Analysis Toolkit Best Practices Pipeline. Current Protocols in Bioinformatics 2013.
9. Ng PC, Henikoff S. SIFT: Predicting amino acid changes that affect protein function. Nucleic Acids Res 2003;31:3812-4.
10. Adzhubei IA, Schmidt S, Peshkin L, et al. A method and server for predicting damaging missense mutations. Nat Methods 2010;7:248-9.
11. Kircher M, Witten DM, Jain P, O'Roak BJ, Cooper GM, Shendure J. A general framework for estimating the relative pathogenicity of human genetic variants. Nat Genet 2014;46:310-5.
12. Gerstel-Thompson JL, Wilkey JF, Baptiste JC, et al. High-throughput multiplexed T-cell-receptor excision circle quantitative PCR assay with internal controls for detection of severe combined immunodeficiency in population-based newborn screening. Clinical chemistry 2010;56:1466-74.
13. Della Chiesa M, Falco M, Bertaina A, et al. Human cytomegalovirus infection promotes rapid maturation of NK cells expressing activating killer Ig-like receptor in patients transplanted with NKG2C-/- umbilical cord blood. J Immunol 2014;192:1471-9.
14. Lim ET, Wurtz P, Havulinna AS, et al. Distribution and medical impact of loss-of-function variants in the Finnish founder population. PLoS Genet 2014;10:e1004494.